

Wavelets in Medical Image Processing: De-noising, Segmentation, and Registration

Yinpeng Jin, Elsa Angelini, and Andrew Laine

**Department of Biomedical Engineering, Columbia University,
New York, NY, USA**

ABSTRACT

Wavelet transforms and other multi-scale analysis functions have been used for compact signal and image representations in de-noising, compression and feature detection processing problems for about twenty years. Numerous research works have proven that space-frequency and space-scale expansions with this family of analysis functions provided a very efficient framework for signal or image data.

The wavelet transform itself offers great design flexibility. Basis selection, spatial-frequency tiling, and various wavelet threshold strategies can be optimized for best adaptation to a processing application, data characteristics and feature of interest. Fast implementation of wavelet transforms using a filter-bank framework enable real time processing capability. Instead of trying to replace standard image processing techniques, wavelet transforms offer an efficient representation of the signal, finely tuned to its intrinsic properties. By combining such representations with simple processing techniques in the transform domain, multi-scale analysis can accomplish remarkable performance and efficiency for many image processing problems.

Multi-scale analysis has been found particularly successful for image de-noising and enhancement problems given that a suitable separation of signal and noise can be achieved in the transform domain (*i.e.* after projection of an observation signal) based on their distinct localization and distribution in the spatial-frequency domain. With better correlation of significant features, wavelets were also proven to be very useful for detection {jin_Mallat_1992a} and matching applications {jin_Strickland_1995}.

One of the most important features of wavelet transforms is their multi-resolution representation. Physiological analogies have suggested that wavelet transforms are similar to low level visual perception. From texture recognition, segmentation to image registration, such multi-resolution analysis gives the possibility of investigating a particular problem at various spatial-frequency (scales). In many cases, a “coarse to fine” procedure can be implemented to improve the computational efficiency and robustness to data variations and noise.

Without trying to cover all the issues and research aspects of wavelet in medical imaging, we focus our discussion in this chapter to three topics: image de-noising/enhancement, image segmentation and image registration using wavelet transforms. We will introduce the wavelet multi-scale analysis framework and summarize related research work in this area and describe recent state-of-the-art techniques.

1. Introduction

Wavelets have been widely used in signal and image processing for the past 20 years. Although a milestone paper by Grossmann and Morlet {jin_Grossman_1984} was considered as the beginning point of modern wavelet analysis, similar ideas and theoretical bases can be found back in early 20th century {jin_Haar_1910}. Following two important papers in late 1980s by S. Mallat {jin_Mallat_1989} and I. Daubechies {jin_Daubechies_1988}, more than 9,000 journal papers and 200 books related to wavelets have been published {jin_Unser_2003a}.

Wavelets were first introduced to medical imaging research in 1991 in a journal paper describing the application of wavelet transforms for noise reduction in MRI images. {jin_Weaver_1991}. Ever since, wavelet transforms have been successfully applied to many topics including tomographic reconstruction, image compression, noised reduction, image enhancement, texture analysis/segmentation and multi-scale registration. Two review papers in 1996 {jin_Unser_1996} and 2000 {jin_Laine_2000} provide a summary and overview of research works related to wavelets in medical image processing from the past few years. Many related works can also be found in the book edited by A. Aldroubi and M. Unser {jin_Aldroubi_1996}. More currently, a special issue of IEEE Transactions on Medical Imaging {jin_Unser_2003a} provides a large collection of most recent research works using wavelets in medical image processing.

The purpose of this chapter is to summarize the usefulness of wavelets in various problems of medical imaging. The chapter is organized as follows. Section 2 overviews the theoretical fundamentals of wavelet theory and related multi-scale representations. As an example, the implementation of an over-complete dyadic wavelet transform will be illustrated. Section 3 includes a general introduction of image de-noising and enhancement techniques using wavelet analysis. Section 4 and 5 will summarize the basic principles and research works in literature for wavelet analysis applied to image segmentation and registration.

2. Wavelet Transform and Multi-scale Analysis

One of the most fundamental problems in signal processing is to find a suitable representation of the data that will facilitate an analysis procedure. One way to achieve this goal is to use transformation, or decomposition of the signal on a set of basis functions prior to processing in the transform domain. Transform theory has played a key role in image processing for a number of years, and it continues to be a topic of interest in theoretical as well as applied work in this field. Image transforms are used widely in many image processing fields, including image enhancement, restoration, encoding, and description {jin_Jain_1989}.

Historically, the Fourier transform has dominated linear time-invariant signal processing. The associated basis functions are complex sinusoidal waves $e^{i\omega t}$ that correspond to the eigenvectors of a linear time-invariant operator. A signal $f(t)$ defined in the temporal domain and its Fourier transform $\hat{f}(\omega)$, defined in the frequency domain, have the following relationships {jin_Jain_1989; jin_Papoulis_1987}:

$$\hat{f}(\omega) = \int_{-\infty}^{+\infty} f(t)e^{-i\omega t} dt, \quad (1)$$

$$f(t) = \frac{1}{2\pi} \int_{-\infty}^{+\infty} \hat{f}(\omega)e^{i\omega t} d\omega. \quad (2)$$

Fourier transform characterizes a signal $f(t)$ via its frequency components. Since the support of the bases function $e^{i\omega t}$ covers the whole temporal domain (i.e infinite support), $\hat{f}(\omega)$ depends on the values of $f(t)$ for all times. This makes the Fourier transform a global transform that cannot analyze local or transient properties of the original signal $f(t)$.

In order to capture frequency evolution of a non-static signal, the basis functions should have compact support in both time and frequency domain. To achieve this goal, a windowed Fourier transform (WFT) was first introduced with the use of a window function $w(t)$ into the Fourier transform {jin_Mallat_1998}:

$$Sf(\omega, t) = \int_{-\infty}^{+\infty} f(\tau)w(t-\tau)e^{-i\omega\tau} d\tau. \quad (3)$$

The energy of the basis function $g_{\tau, \xi}(t) = w(t-\tau)e^{-i\xi t}$ is concentrated in the neighborhood of time τ over an interval of size σ_t , measured by the standard deviation of $|g|^2$. Its Fourier transform is $\hat{g}_{\tau, \xi}(\omega) = \hat{w}(\omega-\xi)e^{-i\tau(\omega-\xi)}$, with energy in frequency domain localized around ξ , over an interval of size σ_ω . In a time-frequency plane (t, ω) , the energy spread of what is called the atom $g_{\tau, \xi}(t)$ is represented by the Heisenberg rectangle with time width σ_t and frequency width σ_ω . The

uncertainty principle states that the energy spread of a function and its Fourier transform cannot be simultaneously arbitrarily small, verifying:

$$\sigma_t \sigma_\omega \geq \frac{1}{2}. \quad (4)$$

Shape and size of Heisenberg rectangles of a windowed Fourier transform therefore determine the spatial and frequency resolution offered by such transform.

Examples of spatial-frequency tiling with Heisenberg rectangles are shown in Figure 1. Notice that for a windowed Fourier transform, the shape of the time-frequency boxes are identical across the whole time-frequency plane, which means that the analysis resolution of a windowed Fourier transform remains the same across all frequency and spatial locations.

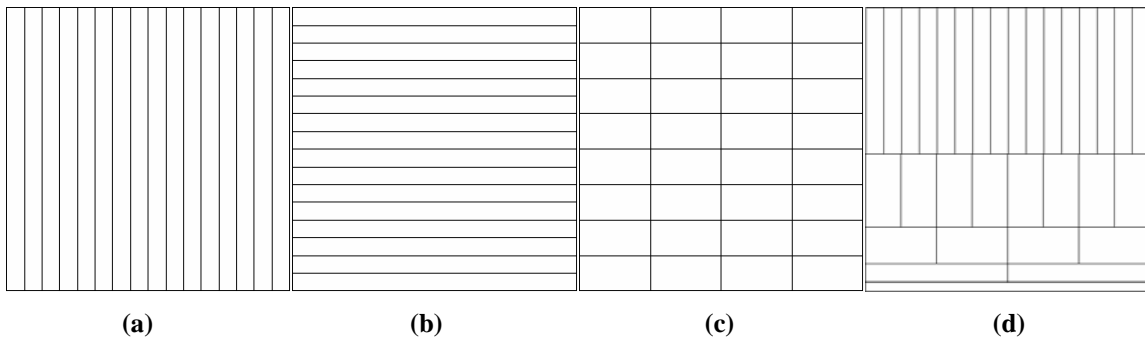


Figure 1: Example of spatial-frequency tiling of various transformations. x-axis: spatial resolution. y-axis: frequency resolution. (a) discrete sampling (no frequency localization). (b) Fourier transform (no temporal localization). (c) windowed Fourier transform (constant Heisenberg boxes). (d) wavelet transform (variable Heisenberg boxes).

To analyze transient signal structures of various supports and amplitudes in time, it is necessary to use time-frequency atoms with different support sizes for different temporal locations. For example, in the case of high frequency structures, which vary rapidly in time, we need higher temporal resolution to accurately trace the trajectory of the changes; on the other hand, for lower frequency, we will need a relatively higher absolute frequency resolution to give a better measurement on the value of frequency. We will show in the next section that wavelet transform provide a natural representation which satisfies these requirements, as illustrated in Figure 1 (d).

2.1 Continuous Wavelet Transform

A wavelet function is defined as a function $\psi \in L^2(\mathbb{R})$ with a zero average {jin_Grossman_1984; jin_Mallat_1998}:

$$\int_{-\infty}^{+\infty} \psi(t) dt = 0. \quad (5)$$

It is normalized $\|\psi\| = 1$, and centered in the neighborhood of $t = 0$. A family of time-frequency atoms is obtained by scaling ψ by s and translating it by u :

$$\psi_{u,s}(t) = \frac{1}{\sqrt{s}} \psi\left(\frac{t-u}{s}\right). \quad (6)$$

A continuous wavelet transform decomposes a signal over dilated and translated wavelet functions. The wavelet transform of a signal $f \in L^2(\mathbb{R})$ at time u and scale s is performed as:

$$Wf(u, s) = \langle f, \psi_{u,s} \rangle = \int_{-\infty}^{+\infty} f(t) \frac{1}{\sqrt{s}} \psi^*\left(\frac{t-u}{s}\right) dt = 0 \quad (7)$$

Assuming that the energy of $\hat{\psi}(\omega)$ is concentrated in a positive frequency interval centered at η , the time-frequency support of a wavelet atom $\psi_{u,s}(t)$ is symbolically represented by a Heisenberg rectangle centered at $(u, \eta/s)$, with time and frequency supports spread proportional to s and $1/s$ respectively. When s varies, the height and width of the rectangle change but its area remains constant, as illustrated by Figure 1 (d).

For the purpose of multi-scale analysis, it is often convenient to introduce the scaling function ϕ , which is an aggregation of wavelet functions at scales larger than 1. The scaling function ϕ and the wavelet function ψ are related through the following relations:

$$|\hat{\phi}(\omega)|^2 = \int_1^{+\infty} |\hat{\psi}(s\omega)|^2 \frac{ds}{s} \quad (8)$$

The low-frequency approximation of a signal f at the scale s is computed as:

$$Lf(u, s) = \langle f(t), \phi_s(t-u) \rangle, \quad (9)$$

with

$$\phi_s(t) = \frac{1}{\sqrt{s}} \phi\left(\frac{t}{s}\right). \quad (10)$$

For a one-dimensional signal f , the continuous wavelet transform (7) is a two-dimensional representation. This indicates the existence of redundancy that can be reduced and even removed by sub-sampling the scale parameter s and translation parameter u .

An orthogonal (non-redundant) wavelet transform can be constructed constraining the dilation parameter to be discretized on an exponential sampling with a fixed dilation steps and the translation parameter by integer multiples of a dilation dependent step [jin_Daubechies_1992].

In practice, it is convenient to follow a dyadic scale sampling where $s = 2^i$ and $u = 2^i \cdot k$, with i and k integers. With dyadic dilation and scaling, the wavelet basis function, defined as:

$$\left\{ \psi_{j,n}(t) = \frac{1}{\sqrt{2^j}} \psi\left(\frac{t - 2^j n}{2^j}\right) \right\}_{(j,n) \in \mathbb{Z}^2}$$

form an orthogonal basis of $L^2(\mathbb{R})$.

For practical purpose, when using orthogonal basis functions, the wavelet transform defined in Equation (7) is only computed for a finite number of scales (2^J) with $J=0, \dots, N$, and a low frequency component $Lf(u, 2^J)$ (often referred to as the DC component) is added to the set of projection coefficients corresponding to scales larger than 2^J for a complete signal representation.

In medical image processing applications, we usually deal with discrete data. We will therefore focus the rest of our discussion on discrete wavelet transform rather than continuous ones.

2.2 Discrete Wavelet Transform and Filter Bank

Given a 1-D signal of length N , $\{f(n), n=0, \dots, N-1\}$, the discrete orthogonal wavelet transform can be organized as a sequence of discrete functions according to the scale parameter $s = 2^j$:

$$\{L_J f, \{W_j f\}_{j \in [1, J]}\} \quad (11)$$

where $L_J f = Lf(2^J n, 2^J)$ and $W_j f = Wf(2^j n, 2^j)$.

Wavelet coefficients $W_j f$ at scale $s = 2^j$ have a length of $N/2^j$ and the largest decomposition depth J is bounded by the signal length N as $(\sup(J) = \log_2 N)$.

For fast implementation (such as filter bank algorithms), a pair of conjugate mirror filters (CMF) h and g can be constructed from the scaling function ϕ and wavelet function ψ as follows:

$$h[n] = \langle \frac{1}{\sqrt{2}} \phi(\frac{t}{2}), \phi(t-n) \rangle \text{ and } g[n] = \langle \frac{1}{\sqrt{2}} \psi(\frac{t}{2}), \phi(t-n) \rangle \quad (12)$$

A conjugate mirror filter k satisfies the following relation:

$$\left| \hat{k}(\omega) \right|^2 + \left| \hat{k}(\omega + \pi) \right|^2 = 2 \text{ and } \hat{k}(0) = 2 \quad (13)$$

It can be proven that h is a low-pass filter, and g is a high-pass filter. The discrete orthogonal wavelet decomposition in Equation (11) can be computed by applying these two filters to the input signal, and recursively decompose the low-pass band, as illustrated in Figure 2. A detailed proof can be found in {jin_Daubechies_1992}.

For orthogonal basis, the input signal can be reconstructed from wavelet coefficients computed in Equation (11) using the same pair of filters, as illustrated in Figure 3.

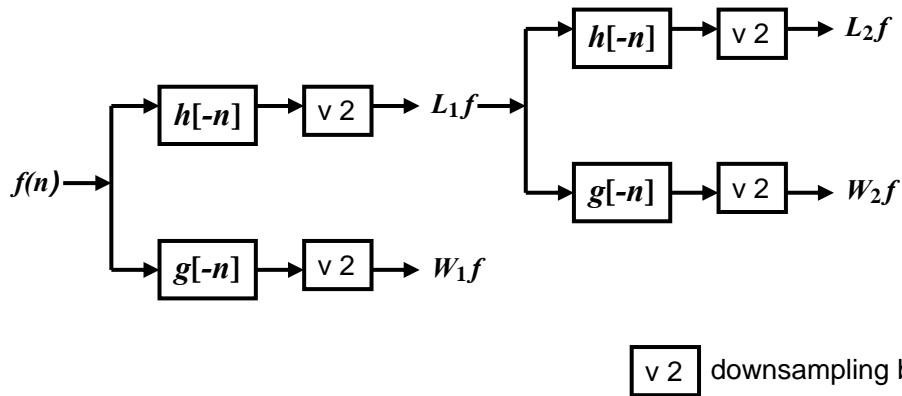


Figure 2: Illustration of orthogonal wavelet transform of a discrete signal $f(n)$ with CMF. A two-level expansion is shown.

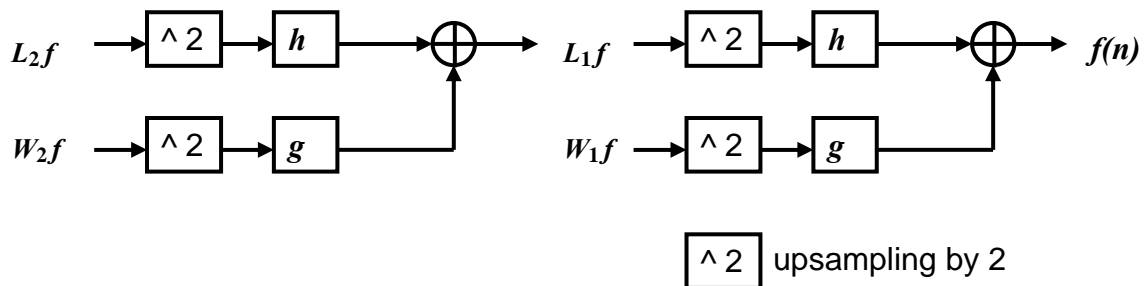


Figure 3: Illustration of inverse wavelet transform implemented with CMF. A two-level expansion is shown.

It is easy to prove that the total amount of data after a discrete wavelet expansion as shown in Figure 2 has the same length to the input signal. Therefore, such transform provides a compact representation of the signal suited for data compression as wavelet transform provides a better spatial-frequency localization. On the other hand, since the data was downsampled at each level of expansion, such transform performs poorly on localization or detection problems. Mathematically, the transform is variant under translation of the signal (i.e. is dependent of the downsampling scheme used during the decomposition), which makes it less attractive for analysis of non-stationary signals. In image analysis, translation invariance is critical to preserve all the information of the signal and a redundant representation needs to be applied.

In the dyadic wavelet transform framework proposed by Mallat and Zhong {jin_Mallat_1992b}, sampling of the translation parameter was performed with the same sampling period as the input signal to preserve translation invariance.

A more general framework of wavelet transform can be designed with different reconstruction and decomposition filters that form a bi-orthogonal basis. Such generalization provides more flexibility in the design of the wavelet functions. In that case, similarly to Equation (11), the discrete dyadic wavelet transform of a signal $s(n)$ is defined as a sequence of discrete functions

$$\{S_M s(n), \{W_m s(n)\}_{m \in [1, M]}\}_{n \in \mathbb{Z}}, \quad (14)$$

where $S_M s(n) = s * \phi_M(n)$ represents the DC component, or the coarsest information from the input signal.

Given a pair of wavelet function $\psi(x)$ and reconstruction function $\chi(x)$, the discrete dyadic wavelet transform (decomposition and reconstruction) can be implemented with a fast filter bank scheme using a pair of decomposition filters H , G and a reconstruction filter K {jin_Mallat_1992b}.

$$\begin{aligned} \hat{\phi}(2\omega) &= e^{-i\omega s} H(\omega) \hat{\phi}(\omega), \\ \hat{\psi}(2\omega) &= e^{-i\omega s} G(\omega) \hat{\psi}(\omega), \\ \hat{\chi}(2\omega) &= e^{i\omega s} K(\omega) \hat{\chi}(\omega). \end{aligned} \quad (15)$$

where s is a $\psi(x)$ dependent sampling shift. The three filters satisfy:

$$|H(\omega)|^2 + G(\omega)K(\omega) = 1. \quad (16)$$

Defining $F_s(\omega) = e^{-i\omega s} F(\omega)$, where F is either H , G or K , we can construct a filter bank implementation of the discrete dyadic wavelet transform as illustrated in Figure 4. Filters $F(2^m \omega)$ defined at level $m+1$ (i.e., filters applied at wavelet scale 2^m) are constructed by

inserting $2^m - 1$ zeros between subsequent filter coefficients from level 1 ($F(\omega)$). Non-integer shifts at level 1 are rounded to the nearest integer. This implementation design is called “algorithme à trous” [jin_Holschneider_1989; jin_Shensa_1992], and has a complexity that increases linearly with the number of analysis levels.

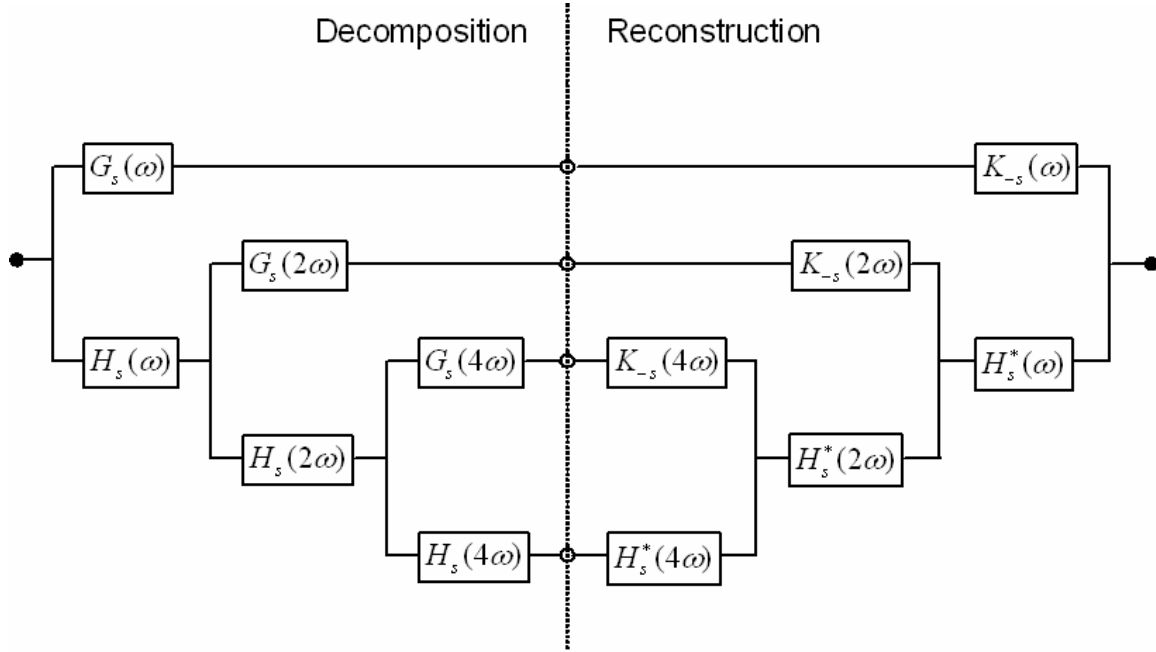


Figure 4: Filter bank implementation of a one-dimensional discrete dyadic wavelet transform decomposition and reconstruction for three levels of analysis. $H_s^*(\omega)$ denotes the complex conjugate of $H_s(\omega)$.

In image processing applications, we often deal with two, three or even higher dimensional data. Extension of the framework to higher dimension is quite straightforward. Multi-dimensional wavelet bases can be constructed with tensor products of separable basis functions defined along each dimension. In that context, a N -D discrete dyadic wavelet transform with M analysis levels is represented as a set of wavelet coefficients:

$$\left\{ S_M s, \{ W_m^1 s, W_m^2 s, \dots, W_m^N s \}_{m=[1, M]} \right\} \quad (17)$$

where $W_m^k = \langle s, \psi_m^k \rangle$ represents the detailed information along the k th coordinate at scale m .

The wavelet basis is dilated and translated from a set of separable wavelet functions $\psi^k, k = 1, \dots, N$ as for example in 3D:

$$\psi_{m,n_1,n_2,n_3}^k(x, y, z) = \frac{1}{2^{3m/2}} \psi^k\left(\frac{x-n_1}{2^m}, \frac{y-n_2}{2^m}, \frac{z-n_3}{2^m}\right), \quad k = 1, 2, 3. \quad (18)$$

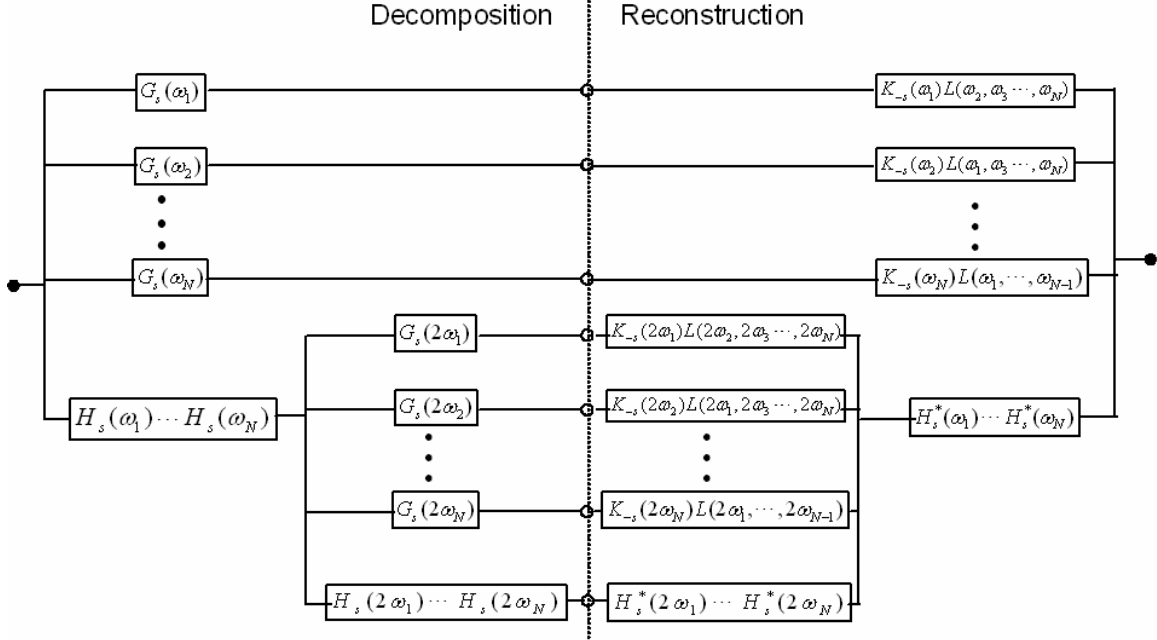


Figure 5: Filter bank implementation of a multi-dimensional discrete dyadic wavelet transform decomposition (left) and reconstruction (right) for two levels of analysis.

In this framework, reconstruction with a N -D dyadic wavelet transform requires a non-separable filter L_N to compensate the inter-dimension correlations. This is formulated in a general context as:

$$\sum_{l=1}^N K(\omega_l)G(\omega_l)L_N(\omega_1, \dots, \omega_{l-1}, \omega_{l+1}, \dots, \omega_N) + \prod_{l=1}^N |H(\omega_l)|^2 = 1 \quad (19)$$

Figure 5 illustrates a filter bank implementation with a multi-dimensional discrete dyadic wavelet transform. For more details and discussions we refer to {jin_Koren_1998}.

2.3 Other Multi-scale Representations

Wavelet transforms are part of a general framework of multi-scale analysis. Various multi-scale representations have been derived from the spatial-frequency framework offered by wavelet expansion, many of which introduced to provide more flexibility for the spatial-frequency selectivity or better adaptation to real world applications.

In this section, we briefly review several multi-scale representations derived from wavelet transforms. Readers with intention to investigate more theoretical and technical details are referred to the text books on Gabor analysis {jin_Feichtinger_1998}, wavelet packets {jin_Wickerhauser_1993}, and the original paper on brushlet {jin_Meyer_1997}.

2.3.1 Gabor Transform and Gabor Wavelets

In his early work, D. Gabor {jin_Gabor_1946} suggested an expansion of a signal $s(t)$ in terms of time-frequency atoms $g_{m,n}(t)$ defined as.

$$s(t) = \sum_{m,n} c_{m,n} g_{m,n}(t), \quad (20)$$

where $g_{m,n}(t)$, $m, n \in Z$ are constructed with a window function $g(x)$, combined to a complex exponential:

$$g_{m,n}(t) = g(t - na)e^{i2\pi mbt}. \quad (21)$$

D. Gabor also suggested that an appropriate choice for the window function $g(x)$ is the Gaussian function due to the fact that a Gaussian function has the theoretically best joint spatial-frequency resolution (uncertainty principle). It is important to note here that the Gabor elementary functions $g_{m,n}(t)$ are not orthogonal and therefore require a bi-orthogonal dual function $\gamma(x)$ for reconstruction {jin_Bastiaans_1981}. This dual window function is used for the computation of the expansion coefficients $c_{m,n}$ as:

$$c_{m,n} = \int f(x)\bar{\gamma}(x-na)e^{-i2\pi mbx} dx, \quad (22)$$

while the Gaussian window is used for the reconstruction.

The biorthogonality of the two window functions $\gamma(x)$ and $g(x)$ is expressed as:

$$\int g(x)\bar{\gamma}(x-na)e^{-i2\pi mbx} dx = \delta_m \delta_n. \quad (23)$$

From Equation (21), it is easy to see that all spatial-frequency atom $g_{m,n}(t)$ share the same spatial-frequency resolution defined by the Gaussian function $g(x)$. As pointed out in the discussion on short-time Fourier transforms, such design is sub-optimal for the analysis of signals with different frequency components.

A wavelet-type generalization of Gabor expansion can be constructed such that different window functions are used instead of a single one {jin_Porat_1988} according to their spatial-frequency location. Following the design of wavelets, a Gabor wavelet $\psi(x) = g(t)e^{im}$ is then obtained with

a Gaussian function $g(t) = \frac{1}{(\sigma^2\pi)^{1/4}} e^{-\frac{t^2}{2\sigma^2}}$ {jin_Mallat_1998}.

Extension of Gabor wavelet to 2-D is expressed as:

$$\psi^k(x, y) = g(x, y)e^{-i\eta(x\cos\alpha_k + y\sin\alpha_k)}. \quad (24)$$

Different translation and scaling parameters of $\psi^k(x, y)$ constitute the wavelet basis for expansion. An extra parameter α_k provides selectivity for the orientation of the function. We observe here that the 2-D Gabor wavelet has a non-separable structure that provides more flexibility on orientation selection than separable wavelet functions.

It is well known that optical sensitive cells in animal's visual cortex respond selectively on stimuli with particular frequency and orientation {jin_Hubel_1962}. Equation (24) described a wavelet representation that naturally reflects this neuro-physiological phenomenon. Gabor

expansion and Gabor wavelets have therefore been widely used for visual discrimination tasks and especially texture recognition {jin_Daugman_1988; jin_Porat_1989}.

2.3.2 Wavelet Packets

Unlike dyadic wavelet transform, wavelet packets decompose the low frequency component as well as the high frequency component in every sub-bands {jin_Coifman_1992}. Such adaptive expansion can be represented with binary trees where each sub-band high or low frequency component is a node with two children corresponding to the pair of high and low frequency expansion at the next scale. An admissible tree for an adaptive expansion is therefore defined as a binary tree where each node has either 0 or 2 children, as illustrated in Figure 6 (c). The number of all different wavelet packet orthogonal basis (also called a wavelet packets dictionary) equals to the number of different admissible binary trees, which is of the order of 2^{2^J} , where J is the depth of decomposition {jin_Mallat_1998}.

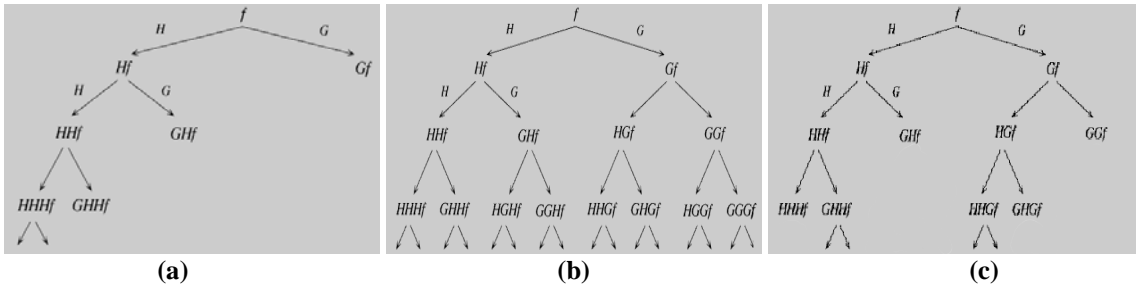


Figure 6: (a) Dyadic wavelet decomposition tree. (b) Wavelet packets decomposition tree. (c) An example of an orthogonal basis tree with wavelet packets decomposition.

Obviously, wavelet packets provide more flexibility on partitioning the spatial-frequency domain, and therefore improve the separation of noise and signal into different sub-bands in an approximated sense (this is referred to the near-diagonalization of signal and noise). This property can greatly facilitate the enhancement and de-noising task of a noisy signal if the wavelet packets basis are selected properly {jin_Coifman_1995b}. In practical applications for various medical

imaging modalities and applications, features of interest and noise properties have significantly different characteristics that can be efficiently characterized separately with this framework.

A fast algorithm for wavelet-packets best basis selection was introduced by Coifman and Wickerhauser in [jin_Coifman_1995b]. This algorithm identifies the “best” basis for a specific problem inside the wavelet packets dictionary according to a criterion (referred to as a cost function) that is minimized. This cost function typically reflects the entropy of the coefficients or the energy of the coefficients inside each sub-band and the optimal choice minimizes the cost function comparing values at a node and its children. The complexity of the algorithm is $O(N \log N)$ for a signal of N samples.

2.3.3 Brushlets

Brushlet functions were introduced to build an orthogonal basis of transient functions with good time-frequency localization. For this purpose, lapped orthogonal transforms with windowed complex exponential functions, such as Gabor functions, have been used for many years in the context of sine-cosine transforms [jin_Malvar_1990].

Brushlet functions are defined with true complex exponential functions on sub-intervals of the real axis as:

$$u_{j,n}(x) = b_n(x - c_n)e_{j,n}(x) + v(x - a_n)e_{j,n}(2a_n - x) - v(x - a_{n+1})e_{j,n}(2a_{n+1} - x) \quad (25)$$

where $l_n = a_{n+1} - a_n$ and $c_n = l_n / 2$. The two window functions b_n and v are derived from the ramp function r :

$$r(t) = \begin{cases} 0 & \text{if } t \leq -1 \\ 1 & \text{if } t \geq 1 \end{cases}, \quad (26)$$

and

$$r^2(t) + r^2(-t) = 1, \forall t \in \mathbb{R}. \quad (27)$$

The bump function v is defined as:

$$v(t) = r\left(\frac{t}{\varepsilon}\right) r\left(\frac{-t}{\varepsilon}\right), t \in [-\varepsilon, \varepsilon]. \quad (28)$$

The bell function b_n is defined by:

$$b_n(t) = \begin{cases} r^2\left(\frac{t+l_n/2}{\varepsilon}\right) & \text{if } t \in [-l_n/2-\varepsilon, -l_n/2+\varepsilon] \\ 1 & \text{if } t \in [-l_n/2+\varepsilon, l_n/2-\varepsilon] \\ r^2\left(\frac{l_n/2-t}{\varepsilon}\right) & \text{if } t \in [l_n/2-\varepsilon, l_n/2+\varepsilon] \end{cases}. \quad (29)$$

An illustration of the windowing functions is provided in Figure 7.

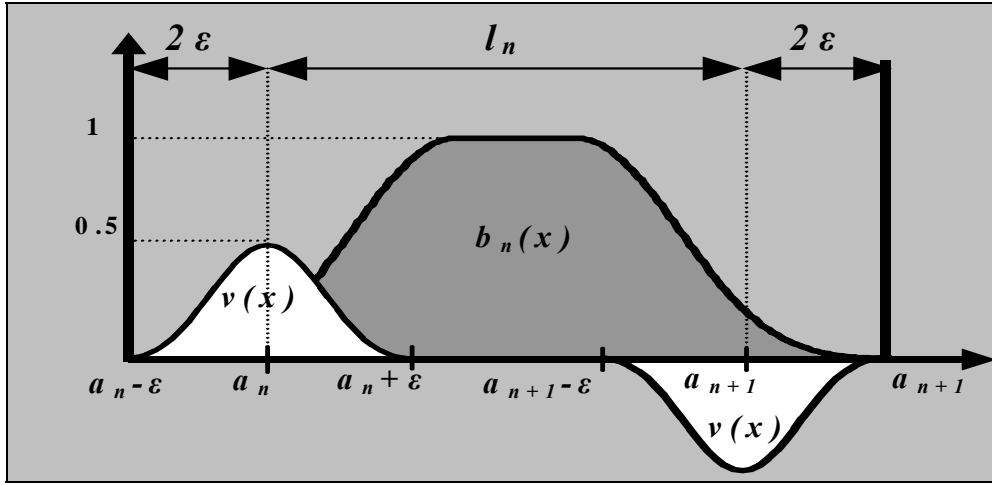


Figure 7: Windowing functions b_n and bump functions v defined on the interval $[a_n - \varepsilon, a_{n+1} + \varepsilon]$.

Finally, the complex-valued exponentials $e_{j,n}$ are defined as:

$$e_{j,n}(x) = \frac{1}{\sqrt{l_n}} e^{-2i\pi j \frac{(x-a_n)}{l_n}}. \quad (30)$$

In order to decompose a given signal f along directional texture components the Fourier transform

\hat{f} of the signal and not the signal itself is projected on the brushlet basis functions:

$$\hat{f} = \sum_n \sum_j \hat{f}_{n,j} u_{n,j}, \quad (31)$$

with $u_{n,j}$ the brushlet basis functions and $\hat{f}_{n,j}$ the brushlet coefficients.

The original signal f can then be reconstructed by:

$$f = \sum_n \sum_j \hat{f}_{n,j} w_{n,j}, \quad (32)$$

where $w_{n,j}$ is the inverse Fourier transform of $u_{n,j}$, which is expressed as:

$$w_{n,j}(x) = \sqrt{l_n} e^{2i\pi a_n x} e^{i\pi l_n x} \left\{ (-1)^j \hat{b}_n(l_n x - j) - 2i \sin(\pi l_n x) \hat{v}(l_n x + j) \right\}, \quad (33)$$

with \hat{b}_n and \hat{v} the Fourier transforms of the window functions b_n and v . Since the Fourier operator is a unitary operator, the family of functions $w_{n,j}$ is also an orthogonal basis of the real axis. We observe here the wavelet-like structure of the $w_{n,j}$ functions with scaling factor l_n and translation factor j . An illustration of the brushlet analysis and synthesis functions is provided in Figure 8, below.

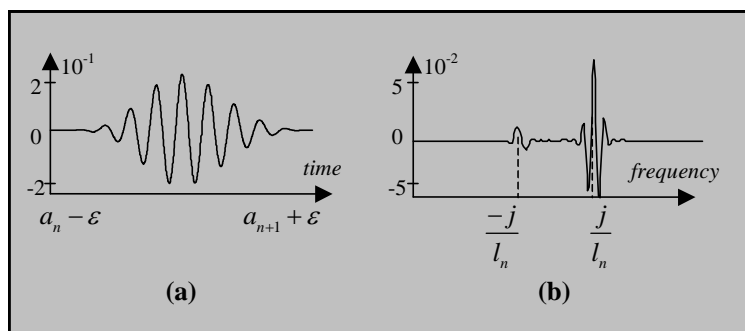


Figure 8: (a) Real part of analysis brushlet function $u_{n,j}$. (b) Real part of synthesis brushlet function

$w_{n,j}$.

Projection on the analysis functions $u_{n,j}$ can be implemented efficiently by a folding operator and Fourier transform (FT). The folding technique was introduced by Malvar {jin_Malvar_1990} and is described for multidimensional implementation by Wickerhauser in {jin_Wickerhauser_1993}.

These brushlet functions share many common properties with Gabor wavelets and Wavelet packets regarding the orientation and frequency selection of the analysis but only brushlet can offer an orthogonal framework with a single expansion coefficient for a particular pair of frequency and orientation.

3. Noise Reduction and Image Enhancement Using Wavelet Transforms

De-noising can be viewed as an estimation problem trying to recover a true signal component X from an observation Y where the signal component has been degraded by a noise component N :

$$Y = X + N. \quad (34)$$

The estimation is computed with a thresholding estimator in an orthonormal basis $\mathbf{B} = \{g_m\}_{0 \leq m < N}$ as {jin_Donoho_1994b}:

$$\hat{X} = \sum_{m=0}^{N-1} \rho_m(\langle X, g_m \rangle) g_m \quad (35)$$

where ρ_m is a thresholding function that aims at eliminating noise components (via attenuating or decreasing some coefficient sets) in the transform domain while preserving the true signal coefficients. If the function ρ_m is modified to rather preserve or increase coefficient values in the transform domain, it is possible to enhance some features of interest in the true signal component with the framework of Equation (35).

Figure 9 illustrates a multi-scale enhancement and de-noising framework using wavelet transforms. An over-complete dyadic wavelet transform using bi-orthogonal basis is used. Notice that since the DC-cap contains the overall energy distribution, it is usually kept untouched during the procedure. As shown in this figure, thresholding and enhancement functions can be implemented independently from the wavelet filters and easily incorporated into the filter bank framework.

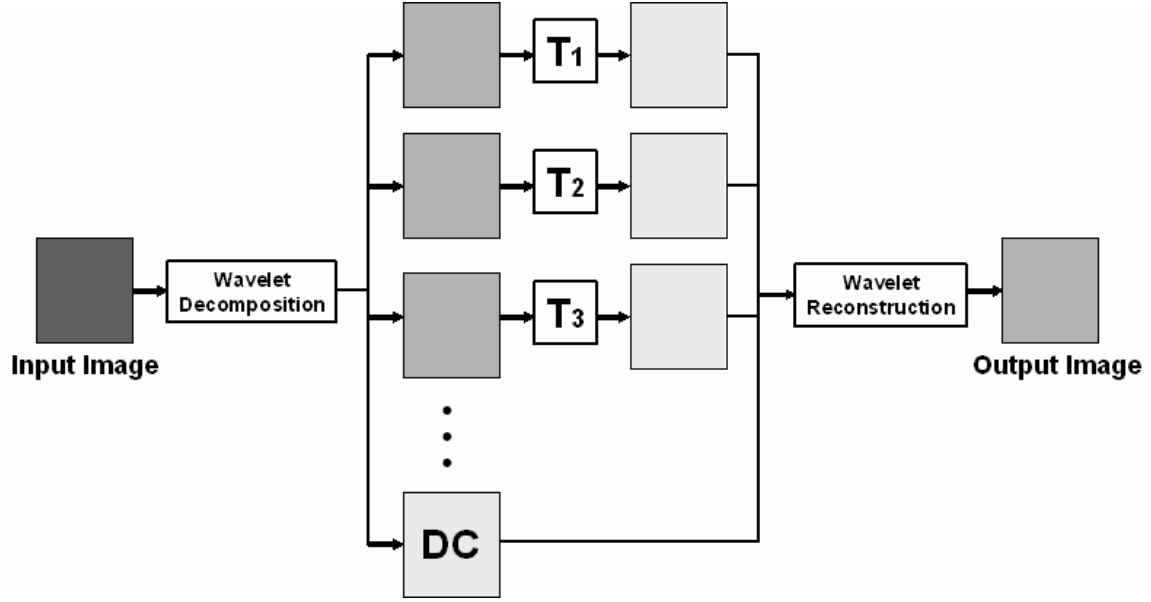


Figure 9: A Multi-scale framework of de-noising and enhancement using discrete dyadic wavelet transform. A three level decomposition was shown.

3.1 Thresholding operators for de-noising

As a general rule, wavelet coefficients with larger magnitude are correlated with salient features in the image data. In that context, de-noising can be achieved by applying a thresholding operator to the wavelet coefficients (in the transform domain) followed by reconstruction of the signal to the original image (spatial) domain.

Typical threshold operators for de-noising include *hard thresholding*:

$$\rho_T(x) = \begin{cases} x, & \text{if } |x| > T \\ 0, & \text{if } |x| \leq T \end{cases}; \quad (36)$$

soft thresholding (wavelet shrinkage) {jin_Donoho_1995b}:

$$\rho_T(x) = \begin{cases} x - T, & \text{if } x \geq T \\ x + T, & \text{if } x \leq -T \\ 0, & \text{if } |x| < T \end{cases}; \quad (37)$$

and *affine(firm) thresholding* {jin_Gao_1997}:

$$\rho_T(x) = \begin{cases} x, & \text{if } |x| \geq T \\ 2x+T, & \text{if } -T \leq x \leq -T/2 \\ 2x-T, & \text{if } T/2 \leq x \leq T \\ 0, & \text{if } |x| < T \end{cases}. \quad (38)$$

The shapes of these thresholding operators are illustrated in Figure 10.

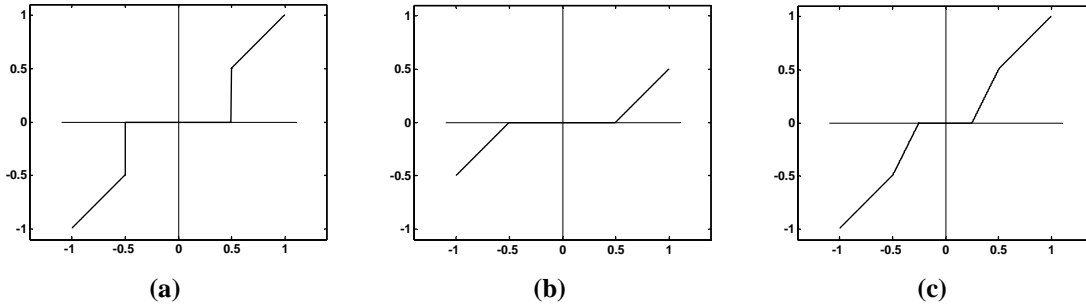


Figure 10: Example of thresholding functions, assuming that the input data was normalized to the range of [-1,1]. (a) Hard thresholding. (b) Soft thresholding. (c) Affine thresholding. The threshold level was set to $T=0.5$;

3.2 Enhancement Operators

Magnitude of wavelet coefficients measures the correlation between the image data and the wavelet functions. For first-derivative based wavelet, the magnitude therefore reflects the “strength” of signal variation. For second-derivative based wavelets, the magnitude is related to the local contrast around a signal variation. In both cases, large wavelet coefficient magnitude occurs around strong edges. To enhance weak edges or subtle objects buried in the background, an enhancement function should be designed such that wavelet coefficients within certain magnitude range were to be amplified.

General guidelines for designing a non-linear enhancement function $E(x)$ are {jin_Laine_1995}:

1. An area of low contrast should be enhanced more than an area of high contrast. This is equivalent to say that smaller values of wavelet coefficients should be assigned larger gains.
2. A sharp edge should not be blurred.

In addition, an enhancement function may be further subjected to the following constraints {jin_Koren_1995}:

1. Monotonically increasing: Monotonicity ensures the preservation of the relative strength of signal variations, and avoids changing location of local extrema, or creating new extrema.
2. Anti-symmetry: ($E(-x) = -E(x)$): This property preserves the phase polarity for “edge crispening”.

A simple piecewise linear function {jin_Laine_1994a} that satisfies these conditions is plotted in Figure 11 (a):

$$E(x) = \begin{cases} x - (K-1)T, & \text{if } x < -T \\ Kx & \text{, if } |x| \leq T \\ x + (K-1)T, & \text{if } x > T \end{cases} \quad (39)$$

Such enhancement is simple to implement, and was used successfully for contrast enhancement on mammograms {jin_Fan_1996; jin_Koren_1998; jin_Laine_1994b}.

From the analysis in previous sub-section, wavelet coefficients with small magnitude were also related to noise. A simple amplification of small magnitude coefficients as performed in Equation (39) will certainly also amplify noise components. This enhancement operator is therefore limited to contrast enhancement of data with very low noise level, such as mammograms or CT images. Such problem can be alleviated by combining the enhancement with a de-noising operator presented in the previous sub-section {jin_Laine_1995}.

A more careful design can provide more reliable enhancement procedures with a control of noise suppression. For example, a sigmoid function {jin_Laine_1994a}, plotted in Figure 11 (b) can be used:

$$E(x) = a[\text{sigm}(c(x-b)) - \text{sigm}(-c(x+b))], \quad (40)$$

where

$$a = \frac{1}{\text{sigm}(c(1-b)) - \text{sigm}(-c(1+b))}, \text{ and } 0 < b < 1,$$

and $\text{sigm}(y)$ is defined as: $\text{sigm}(y) = \frac{1}{1 + e^{-y}}$. The parameters b and c respectively control the threshold and rate of enhancement. It can be easily shown that $E(x)$ in Equation (40) is continuous and monotonically increasing within the interval $[-1, 1]$. Furthermore, any order of derivatives of $E(x)$ exists and is continuous. This property avoids creating any new discontinuities after enhancement.

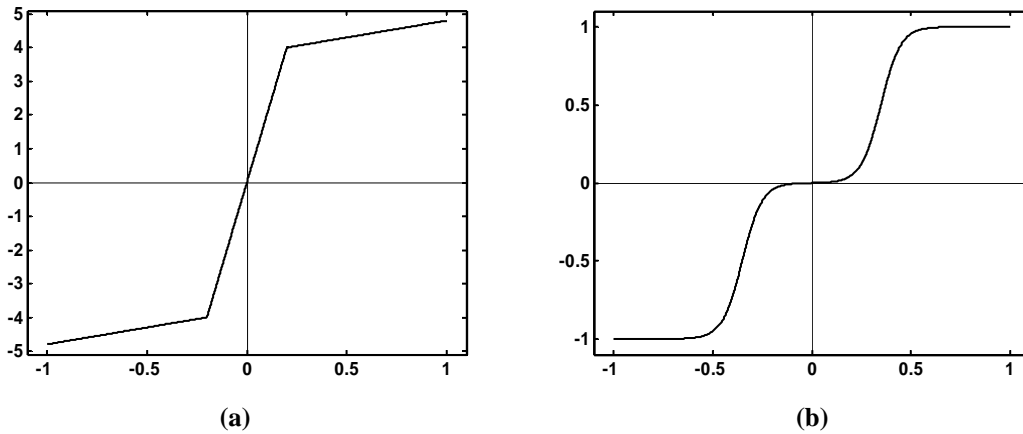


Figure 11: Example of enhancement functions, assuming that the input data was normalized to the range of $[-1,1]$. (a) Piecewise linear function. $T=0.2$, $K=20$. (b) Sigmoid enhancement function. $b=0.35$, $c=20$. Notice the different scales of the y-axis for the two plots.

3.3 Selection of Threshold Value

Given the basic framework of de-noising using wavelet thresholding as discussed in the previous sections, it is clear that the threshold level parameter T plays an essential role. Values too small cannot effectively get rid of noise component, while values too large will eliminate useful signal components. There are a variety of ways to determine the threshold value T as we will discuss in this section.

Depending on whether or not the threshold value T changes across wavelet scales and spatial locations, the thresholding can be:

1. **Global Threshold:** a single value T is to be applied globally to all empirical wavelet coefficients at different scales. $T = \text{const}$.
2. **Level-Dependent Threshold:** a different threshold value T is selected for each wavelet analysis level (scale). $T = T(j)$, $j = 1, \dots, J$. J is the coarsest level for wavelet expansion to be processed.
3. **Spatial Adaptive Threshold:** the threshold value T varies spatially depending on local properties of individual wavelet coefficients. Usually, T is also level-dependent. $T = T_j(x, y, z)$.

While a simple way of determining T is a percentage of coefficients maxima, there are different adaptive ways of assigning the T value according to the noise level (estimated via its variance σ):

1. **Universal Threshold:** $T = \sigma\sqrt{2\log n}$ {jin_Coifman_1995a}, with n equal to the sample size. This threshold was determined in an optimal context for soft thresholding with random Gaussian noise. This scheme is very easy implement, but typically provides a threshold level larger than with other decision criteria, therefore resulting in smoother reconstructed data. Also such estimation does not take into account the content of the data, but only depends on the data size.

2. **Minimax Threshold:** $T = \sigma T_n$ {jin_Donoho_1994a}, where T_n is determined by a minimax rule such that the maximum risk of estimation error across all locations of the data is minimized. This threshold level depends on the noise and signal relationships in the input data.
3. **Stein Unbiased Estimated of Risk (SURE):** Similar as minimax threshold but T_n is determined by a different risk rule {jin_Donoho_1995a; jin_Stein_1981}.
4. **Spatial Adaptive Threshold:** $T = \sigma^2 / \sigma_x$ {jin_Chang_2000}, where σ_x is the local variance of the observation signal, which can be estimated using a local window moving across the image data or, more accurately, by a context-based clustering algorithm.

In many automatic de-noising methods to determine the threshold value T , an estimation of the noise variance σ is needed. Donoho and Johnstone {jin_Donoho_1995c} proposed a robust estimation of noise level σ based on the median absolute value of the wavelet coefficients as:

$$\sigma = \frac{\text{median}(|W_1(x, y, z)|)}{0.6745} \quad (41)$$

where W_1 is the most detailed level of wavelet coefficients. Such estimator has become very popular in practice and is widely used.

3.4 Summary

In general, multi-scale de-noising techniques involve a transformation process and a thresholding operator in the transform domain. Research dedicated on improving such technique has been explored along both directions. Various multi-scale expansions have been proposed aiming at better adaptation to signal and feature characteristics. Traditionally, an orthogonal base was used for expansion {jin_Donoho_1995b}, which leads to a spatial variant transform. Various artifacts, e.g. pseudo-Gibbs phenomena were exhibited in the vicinity of discontinuities. Coifman and Donoho {jin_Coifman_1995a} proposed a translation invariant thresholding scheme, which

averages several de-noising results on different spatial shifts of the input image. Laine *et al.* {jin_Laine_1994b} prompted to an over-complete representation which allows redundancy in the transform coefficients domain, and provides a translation invariant decomposition. Wavelet coefficients in an over-complete representation have the same size as the input image, when treated as a sub-band image. Many de-noising and enhancement techniques can be applied within a multi-scale framework for spatial-frequency adaptation and solve certain noise amplification problems. For a better separation of noise and signal components in the transform domain, other multi-scale representations have also been widely investigated. Examples such other multi-scale representations can be found in previous section 2.3.

The magnitude of the wavelet coefficients is related to the correlations between the signal and the wavelet basis function, which is the only criterion to determine whether or not noise variation appears. Therefore, the selection of the wavelet basis is a critical step in the design of the de-noising and enhancement procedure. Wavelet basis constructed from derivatives of spline functions {jin_Koren_1996} were shown to have many advantages in de-noising and enhancement. Such wavelet functions, either symmetric or anti-symmetric, are smooth with compact support. Higher order spline function resembles Gaussian function, therefore providing ideal spatial-frequency resolution for signal analysis. Moreover, modulus of wavelet coefficients using first derivative spline wavelets are proportional to the magnitude of a gradient vector {jin_Kalifa_2003}. Analysis over such modulus therefore provides extra information on directional correlations, and is especially important for three or higher dimensional data analysis. Other wavelet basis functions have also been developed to provide specific adaptation to different type of signals. To name a few, slantlet {jin_Selesnick_1999}, curvelet {jin_Candes_1999a; jin_Starck_2002}, ridgelet {jin_Candes_1999b} were designed to improve the correlations with edge information, and were used for edge-preserved de-noising, while Fresnelets functions, based on B-spline functions {jin_Liebling_2003}, were designed for processing of digital holography.

In a parallel direction, many research works on multi-scale de-noising focused on improving thresholding operators. In the following discussion, “thresholding operator” is a rather general concept that include both de-noising and enhancement operators as described before. A determination of thresholding method includes both selection of the thresholding operator and a decision or estimation of the threshold parameters (threshold level, enhancement gain etc.). Some examples of thresholding operators designed to improve the basic thresholding rules as shown in Equations (36)-(37)-(38) include the nonnegative garrote thresholding {jin_Gao_1998}:

$$\rho_T^G(x) = \begin{cases} 0, & \text{if } |x| \leq T \\ x - \frac{T^2}{x}, & \text{if } |x| > T \end{cases}, \quad (42)$$

and the SCAD thresholding {jin_Antoniadis_2001; jin_Gao_1998}:

$$\rho_T^{SCAD}(x) = \begin{cases} \text{sign}(x) \max(0, |x| - T), & \text{if } |x| \leq 2T \\ ((\alpha - 1)x - \alpha T \text{sign}(x)) / (\alpha - 2), & \text{if } 2T < |x| \leq \alpha T \\ x, & \text{if } |x| > \alpha T \end{cases}. \quad (43)$$

On the other hand, cross-validation {jin_Jansen_1997; jin_Nason_1996; jin_Weyrich_1995} and recursive hypothesis testing procedure {jin_Ogden_1996} were investigated for automatically determining the threshold level T .

3.5 State-of-the-Arts and Applications:

In this section, we review two examples of multi-scale de-noising. To illustrate the power of multi-scale analysis, two extreme cases of medical imaging modalities (ultrasound and PET/SPECT) with high noise level and complicated noise patterns were considered. A more detailed description of these clinical applications can be found in {jin_Angelini_2001; jin_Jin_2003}.

3.5.1 Spatial-Temporal Analysis of Real Time 3D Cardiac Ultrasound Using Brushlet {jin_Angelini_2001}

Recent development of a real-time three-dimensional (RT3D) ultrasound imaging modality that captures an entire cardiac volume instantaneously with fixed geometric parameters over a complete cardiac cycle raises new issues and challenges for de-noising and volume extraction. On one hand, resolution of RT3D is lower than with previous 2D and 3D generations of ultrasound modalities and the level of speckle noise is very high. On the other hand the amount of information recorded per cardiac cycle is much bigger as this is a true 3D+Time modality. Because of the fast acquisition time and the true three-dimensional nature of the transducer, there exists a strong coherence of surfaces in 3D space and time for echocardiograms recorded from moving cardiac tissue that should be exploited for optimal de-noising and enhancement.

A simple observation of ultrasound images reveal the absence of true boundaries between the blood cavity and the myocardium muscle tissue. The myocardial wall is rather depicted as a field of bright moving texture and the de-noising problem can therefore be approached as a texture characterization task. Approaches for texture classification and de-noising can be divided into structural and statistical methods adapted respectively to macro and micro textural elements. Recent work on texture characterization and more specifically de-noising of ultrasound data via spatio-temporal analysis include steerable filters and Gabor oriented filters {jin_Chen_2001; jin_Mulet-Parada_1998}. Both techniques are non-orthogonal and therefore suffer from non-complete partitioning of the Fourier domain. As we showed in previous section, brushlets allow more flexibility on the partitioning of the Fourier domain and work with an orthogonal basis that provides perfect reconstruction of an original signal. In this application, modifications from the original implementation which extended the analysis to three and four dimensions and performed the analysis in an overcomplete framework have been made.

Brushlet basis functions decompose an n -D signal along specific spatial directions via analysis of

its Fourier domain. As they only depends on spatial frequency content, brushlet decompositions are invariant to the intensity or contrast range in the original data. This makes them very suitable and a powerful basis for the analysis of RT3D ultrasound where choosing a single global intensity-based edge threshold is not possible due to position dependent attenuation of the signal.

There are as many basis functions as there are subintervals in the Fourier domain defining brushstrokes associated with the center frequency of each interval. The tiling of the Fourier domain therefore determines the resolution and orientation of the brushlet basis functions as illustrated in Figure 12 (a).

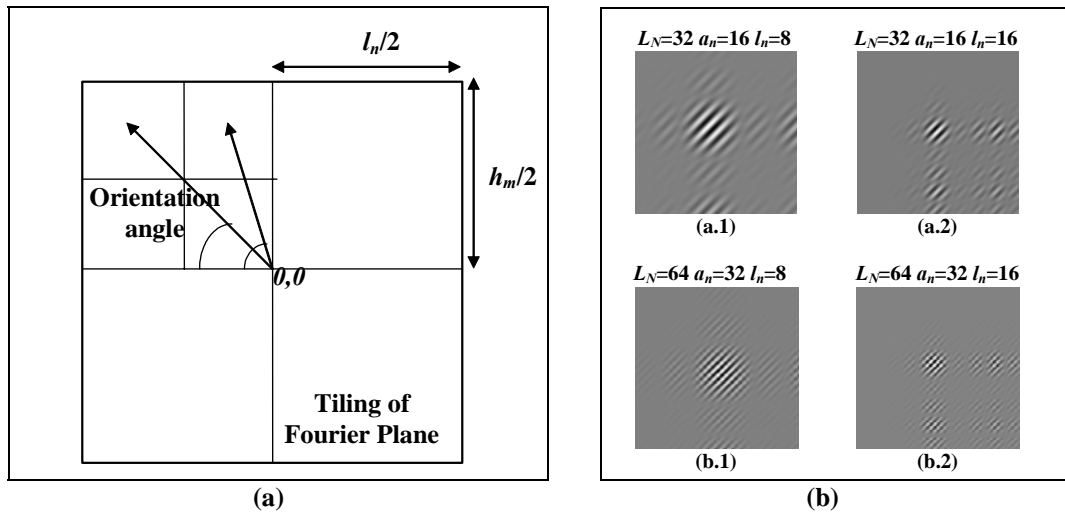


Figure 12: (a) Orientation and oscillation frequency of brushlet analysis functions in 2D. The size of each sub-quadrant in the Fourier plane determines the resolution of the analysis function while the position of the sub-quadrant center determines the orientation of the analysis function. (b) Illustration of selected brushlet orientation and oscillation frequencies. Fourier plane size L_N , center frequency a_n and subintervals size l_n are provided for each 2D brushlet basis function.

The resolution of each brushstroke is inversely proportional to the size of the interval, as illustrated in Figure 12 (b). The major difference between the brushlet basis and wavelet packets is the possibility of any arbitrary tiling of the time-frequency plane and the perfect localization of

a single frequency in one coefficient.

Spatial De-noising via Thresholding

De-noising was performed via thresholding of the brushlet coefficients. In the case of RT3D ultrasound, speckle noise components are concentrated in the high frequency coefficients without specific direction whereas cardiac structures are decomposed in the low frequency components along different orientations. Decorrelation of signal and noise in the frequency domain was therefore performed by removing the higher-frequency components and thresholding only the lower-frequency components prior to reconstruction. De-noising performance was compared for processing in 2D and 3D to demonstrate the advantage of extending the brushlet analysis to 3D as illustrated in Figure 13, below, for a set of six long-axis and six short-axis slices.

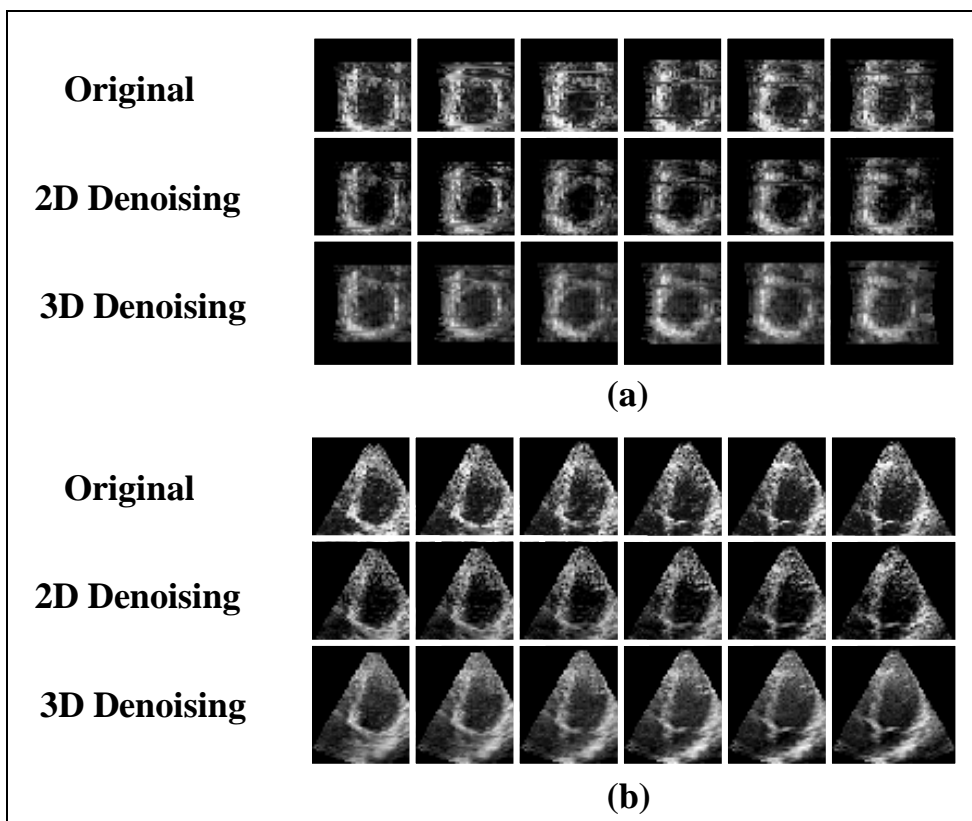


Figure 13: 2D vs. 3D spatial de-noising on RT3D ultrasound data. (a) Series of six consecutive short-axis slices extracted from a clinical data set. (b) Series of six consecutive long-axis slices extracted from the same clinical data set.

Qualitatively, it was observed that the third dimension improved the quality of the de-noised data in terms of spatial resolution at the cost of losing some contrast. When compared to 2D de-noising, 3D de-noising produced smoother features with better-localized contours. Specifically, small local artifacts not persistent in adjacent slices were eliminated and inversely weak contours persistent in adjacent slices were enhanced. This phenomenon can be best appreciated in the short-axis examples where the resolution is the lowest.

Improving De-noising by Including Time: Results on a Mathematical Phantom

To quantitatively evaluate potential de-noising performance improvement brought by including the temporal dimension, initial testing was performed on a mathematical phantom. The phantom, plotted in Figure 14, consisted of an ovoid volume growing in time that schematically mimicked aspects of the left ventricle with an inner gray cavity surrounded by a thick white wall on a black background. The size of a single volume was $64 \times 64 \times 64$ and there were 16 frames growing in time. The volume increased by 70 % over 16 time frames, similar to the average ejection fraction in normal patients.

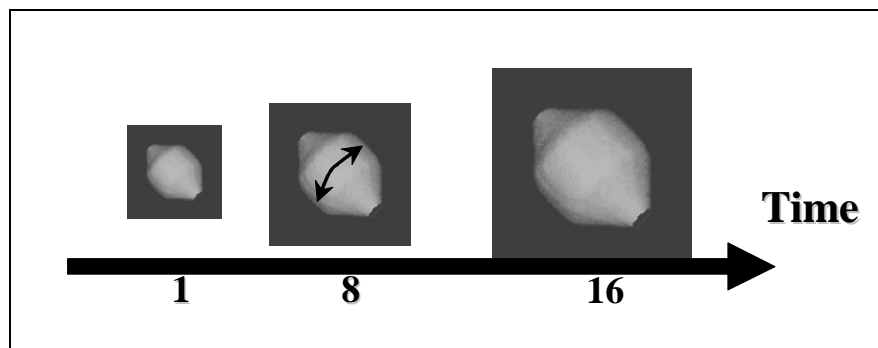


Figure 14: Mathematical phantom. Ovoid volume with 16 frames growing in time.

The phantom was corrupted with two types of noise: (1) Multiplicative speckle noise with uniform distribution, (2) Multiplicative speckle noise with Rayleigh distribution.

The level of speckle noise was set so that the SNR of the noisy data was equal to -15dB. Cross sectional slices through a single volume of the noisy phantoms are displayed in Figure 15.

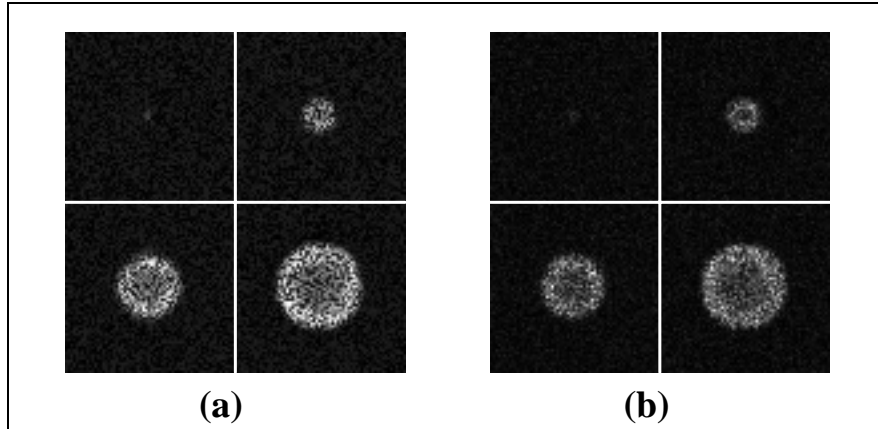


Figure 15: Mathematical phantom corrupted with speckle noise. (a) Speckle noise with uniform distribution. (b) Speckle noise with Rayleigh distribution.

De-noising was carried out with both 3D and 4D brushlet analysis. Regular tiling was applied with four subintervals in each dimension. Volumes were reconstructed after resetting the higher frequency coefficients and hard thresholding the lower frequency coefficients at 25 % of their maxima. Results for a single slice are provided in Figure 16.

These results revealed that including the temporal dimension greatly improved the de-noising performance. From a qualitative point of view, the contrast of the de-noised slices was improved and with a higher definition of borders and more homogeneity inside the white and gray areas. Quantitatively, SNR values were improved by 50 % between 3D and 4D de-noising.

A second motivation for performing multidimensional analysis on cardiac clinical data is to take full advantage of the continuity of spatial and temporal frequency content of multidimensional RT3D signals. The high level of speckle noise in ultrasound clinical data sets recorded with the real-time 3D transducer, the non-uniform absorption coefficients of cardiac tissues and the motion of the heart contribute to the addition of artifacts that can either add echo-like signals inside the cavity or suppress echo signals from the myocardium wall. These artifacts complicate the segmentation task by introducing artificial edges inside the cavity or destroying edges at the epicardial and endocardial borders. Since these artifacts are not persistent in time, including the

temporal component in the analysis helps resolve them. To illustrate the aptitude of the brushlet analysis to repair missing contour information, the previous mathematical phantom was modified by removing a part of the white wall in the eighth time frame. Both 3D analysis on the time frame with the defect and 4D brushlet analysis applied to the sixteen time frames were computed after corruption with Rayleigh speckle noise. Results are displayed in Figure 17, below.

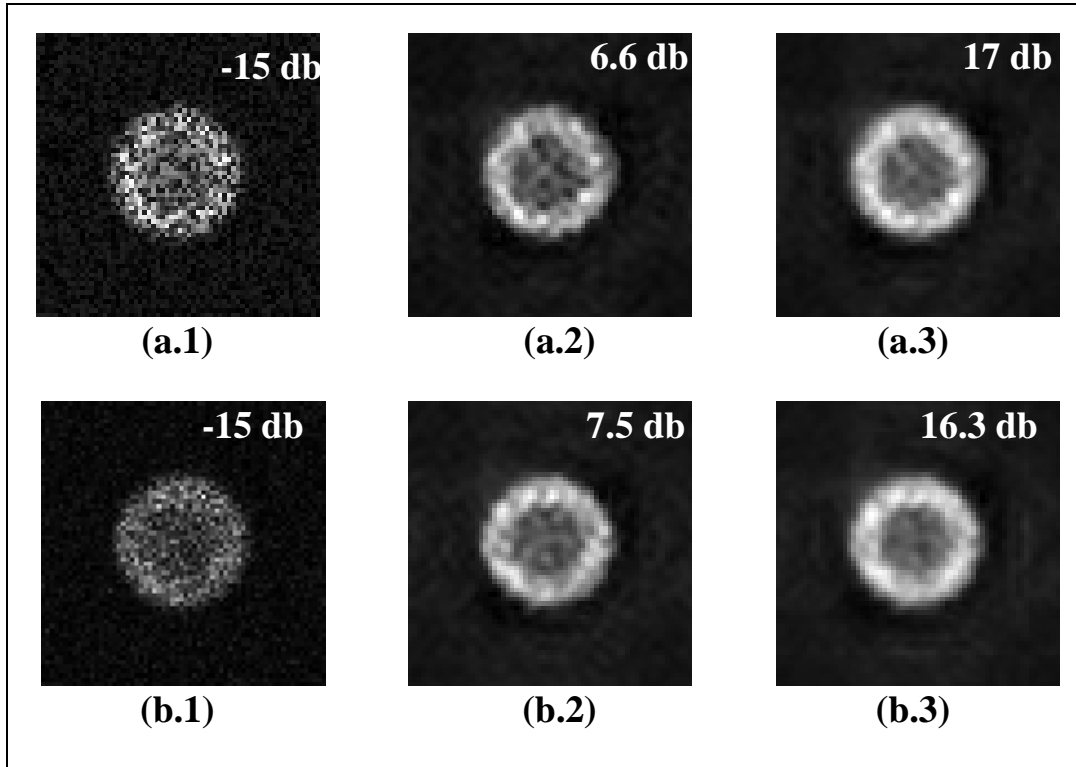


Figure 16: De-noising of mathematical phantom with 3D and 4D brushlet analysis. (a) Results for phantom corrupted with uniformly distributed speckle noise. (b) Results for phantom corrupted with Rayleigh distributed speckle noise. (a.1-b.1) Original slices. (a.2-b.2) Slices de-noised with 3D brushlet expansion. (a.3-b.3) Slices de-noised with 4D brushlet expansion. SNR values are indicated for each slice.

Results showed a remarkable correction of the wall defect with the 4D (3D + time) brushlet de-noising that could not be obtained with 3D analysis alone. This type of artifact is similar to the dropouts in echo signals that result in loss of myocardium tissue in some frames or the

introduction of tissue-like signals inside the cavity. Such artifacts are not persistent in time and could be removed with the inclusion of temporal dimension in the de-noising process.

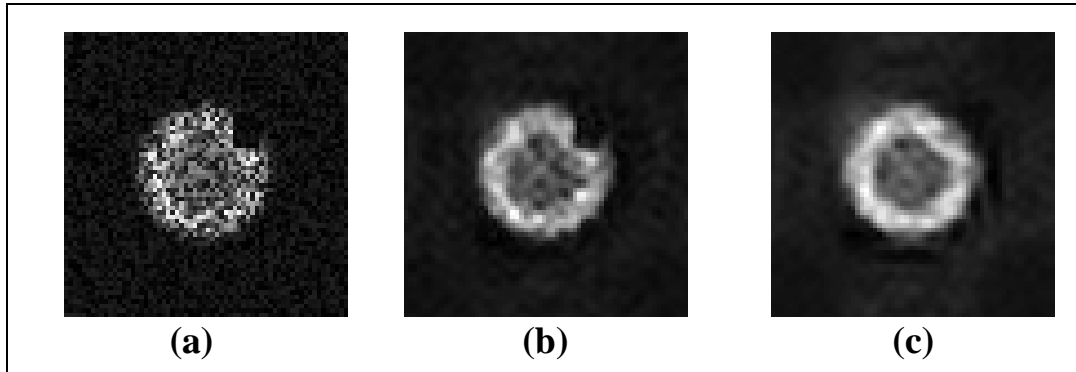


Figure 17: (a) Original noisy slice with defect. (b) De-noised slice with 3D brushlet analysis (c) De-noised slice with 4D brushlet analysis.

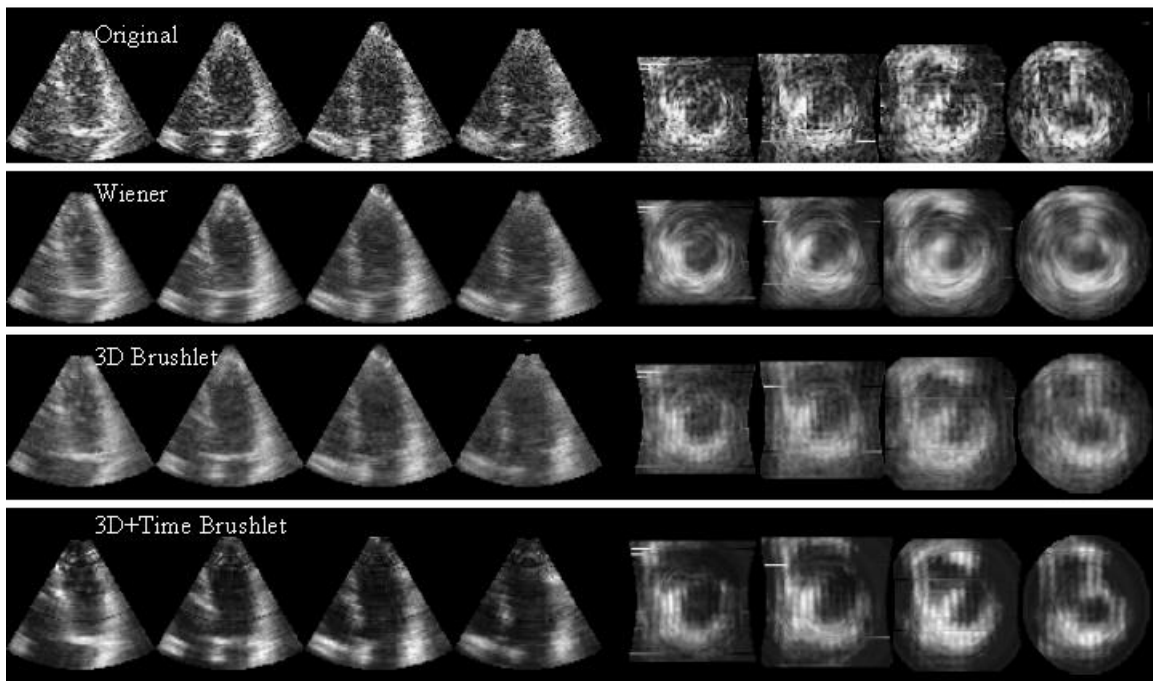


Figure 18: Spatio-temporal de-noising with brushlet expansion on RT3D ultrasound data illustrated on four long axis and four short axis slices.

Finally, experiments on clinical data sets, as illustrated in Figure 18, showed the superior performance of spatio-temporal de-noising versus simple spatial de-noising and Wiener filtering

on RT3D ultrasound data. Adding the time dimension lead to images with better contrast and sharper contours while preserving the original textural aspect of the ultrasound data. Wiener filtering provided good results but introduced blurring artifacts that severely altered the quality of the short-axis de-noised views. This type of artifact is unacceptable in medical applications where anatomical structure detail needs to be preserved. It was also observed that the epicardium borders were enhanced with sharper contrast when combining brushlet spatial and temporal de-noising. Such enhancement is very desirable for quantification of LV mass and wall thickness analysis that require segmentation of both the myocardial endocardial and epicardial borders.

3.5.2 Cross-scale Regularization for Tomographic Images {jin_Jin_2003}

Tomographic image modalities such as PET and SPECT rely on an instable inverse problem of spatial signal reconstruction from sampled line projections. Tomographic reconstruction includes back projection of the sinogram signal via Radon transform and regularization for removal of noisy artifacts. Because the Radon transform is a smoothing process, back projection in the presence of additive noise is an ill-posed inverse problem that requires a regularization of the reconstructed noise component, which can become very large. Standard regularization methods include filtered back-projection (FBP) with non-linear filtering corrections, expectation-maximization (EM) and maximum a posteriori (MAP) estimators {jin_Farquhar_1998; jin_Hudson_1994; jin_McLachlan_1997; jin_Shepp_1982}. The most commonly used tomographic reconstruction method combines a low-pass filter, for noise suppression, and a ramp filter for standard Filtered Back-projection algorithm. The cut-off frequency of the low-pass filter controls the balance between signal-to-noise ratio (SNR) and spatial resolution. While high frequency noise is eliminated after low-pass filtering, useful high frequency information, such as sharp varied signals and edges, are also attenuated. In addition, noise components in low frequency bands still exist. For these two reasons, tomographic images reconstructed with FBP algorithms often suffer from over-smoothness or/and low SNR. Post-processing including de-

noising and enhancement is therefore helpful on improving image qualities for reliable clinical interpretation.

As low-pass filtering has always been considered one of the most fundamental de-noising techniques, embedding a multi-scale de-noising module to partially replace the low-pass filtering operator in the FBP algorithm can potentially improve the image quality of reconstruction in terms of both spatial resolution and signal-to-noise ratio. The intuitive approach to combine FBP and de-noising is therefore to preserve more high-frequency features during the FBP reconstruction, by using a low-pass filter with higher cut-off frequency, or removing the low-pass pre-filtering. The extra amount of noise kept with the high-frequency signal components is then further processed via a multi-scale de-noising operator. An illustration of the de-noising performance is provided in Figure 19 for simple comparison between traditional FBP using a clinical console (Low-pass filter using Hann filter with cut-off frequency set to 0.4), and the proposed two-step processing. It can be observed that the second method, based on FBP using Hann filter with a higher cut-off frequency, generates a reconstructed image containing more detailed information as well as more significant noisy features. After multi-scale de-noising (combining Wavelet Packets thresholding and brushlet thresholding), image quality was markedly improved showing more anatomical details and spatial information.

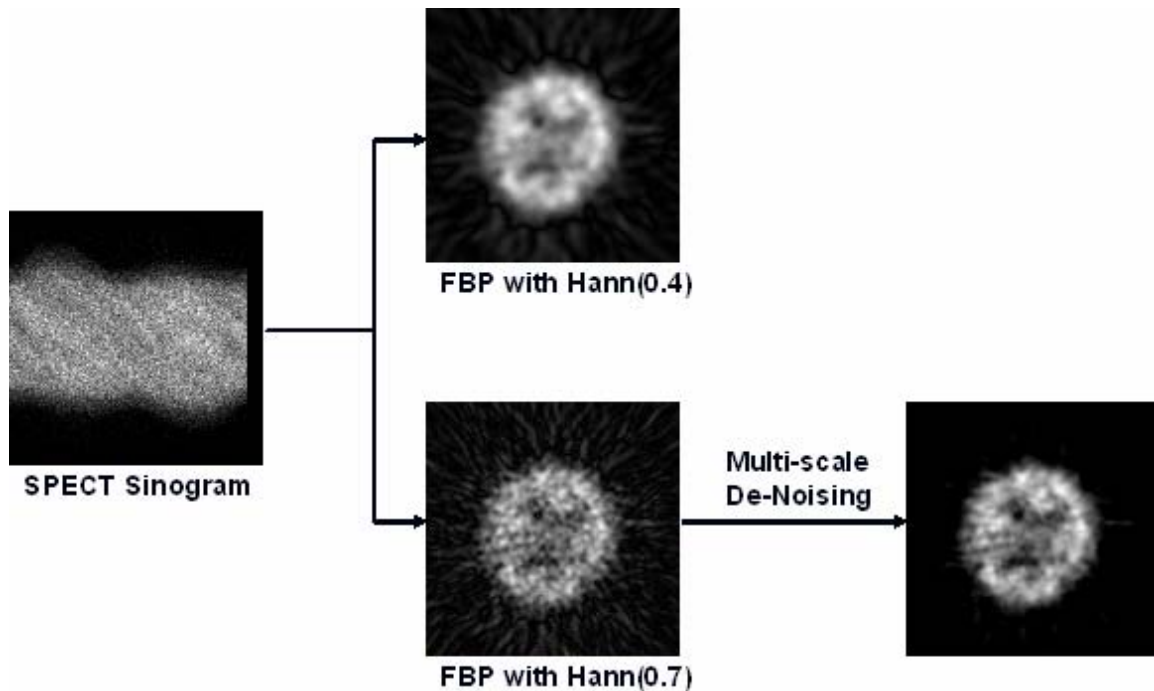


Figure 19: Illustration on a clinical brain SPECT slice of the combination of multi-scale de-noising and traditional FBP with higher cut-off frequency to improve tomographic reconstruction.

Thresholding on Three Dimensional Wavelet Modulus

Both PET and SPECT image reconstructed using FBP display strong directional noise patterns. Most feature-based de-noising methods, including wavelet thresholding, are based on edge information and are not suited for directional noise components that resemble strong edges. Indeed edge information alone cannot accurately separate noise from meaningful signal features in a single image. A novel approach to overcome this limitation is to apply the multi-scale analysis and de-noising scheme using three-dimensional wavelet expansion that integrates edge information along continuous boundaries in 3-D space. In three-dimensions, such integration can accurately separate anatomical surfaces from noisy components that do not exhibit a directional pattern across adjacent tomographic slices. Unlike traditional wavelet de-noising techniques, thresholding was performed on the modulus of the wavelet coefficients (“wavelet modulus”). A first derivative of the cubic spline function was used for the wavelet basis function which

approximates the first derivatives of a Gaussian function and therefore benefits from the following properties:

1. By the uncertainty principle {jin_Mallat_1998}, the Gaussian probability density function is optimally concentrated in both time and frequency domain, and thus is suitable for time-frequency analysis.
2. Derivatives of Gaussian function can be used for rotation-invariant processing {jin_Freeman_1991}.
3. The Gaussian function generates a causal (in a sense that a coarse scale depends exclusively on the previous finer scale) scale space. This make possible scale-space “tracking” of emergent features {jin_Babaud_1986}.

Because the wavelet basis ψ^1, ψ^2, ψ^3 are first derivative of a cubic spline function θ , the three components of a wavelet coefficient $W_m^k s(n_1, n_2, n_3) = \langle s, \psi_{m, n_1, n_2, n_3}^k \rangle, k = 1, 2, 3$ are proportional to the coordinates of the gradient vector of the input image s smoothed by a dilated version of θ . From these coordinates, one can compute the angle of the gradient vector, which indicates the direction in which the first derivative of the smoothed s has the largest amplitude (or the direction in which s changes the most rapidly). The amplitude of this maximized first derivative is equal to the modulus of the gradient vector, and therefore proportional to the wavelet modulus:

$$M_m s = \sqrt{|W_m^1 s|^2 + |W_m^2 s|^2 + |W_m^3 s|^2} \quad (44)$$

Thresholding this modulus value instead of the coefficient value consists of first selecting a direction in which the partial derivative is maximum at each scale, and then thresholding the amplitude of the partial derivative in this direction. The modified wavelet coefficients are then computed from the thresholded modulus and the angle of the gradient vector. Such paradigm applies an adaptive choice of the spatial orientation in order to best correlate the signal features with the wavelet coefficients. It can therefore provide a more robust and accurate selection on

correlated signals comparing to traditional orientation selection along three orthogonal Cartesian directions.

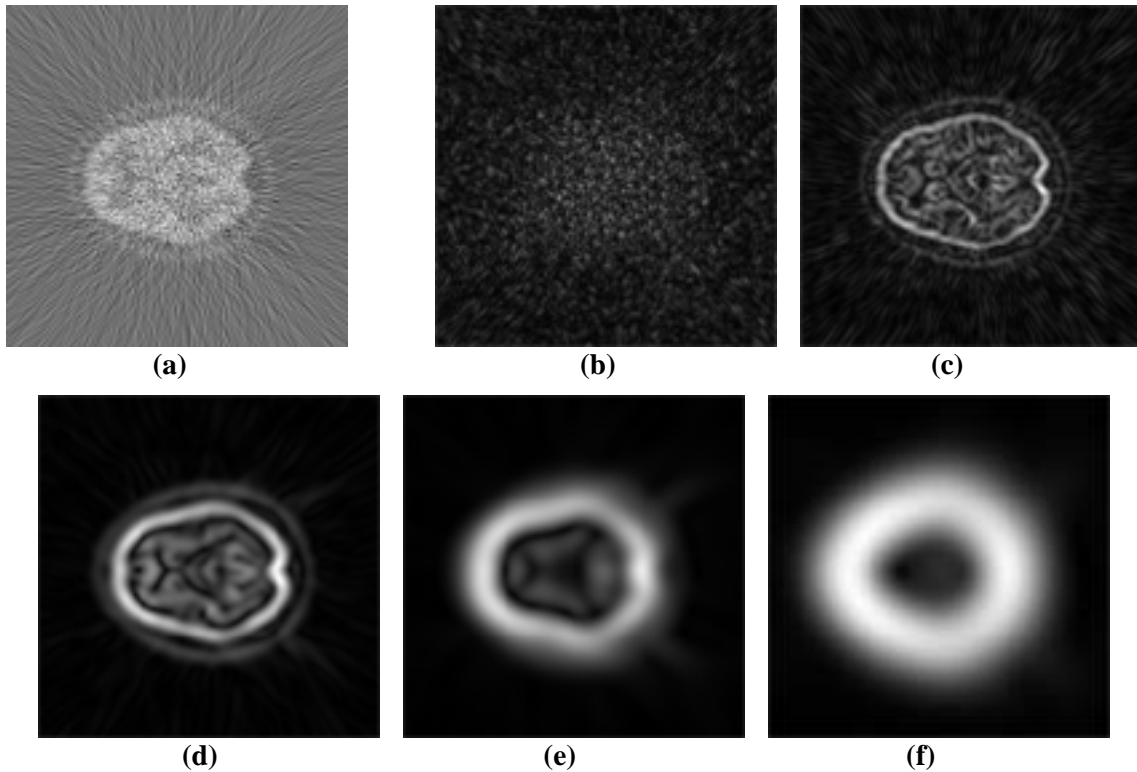


Figure 20: (a) A brain PET image from a 3D data set with high level of noise, (b)~(f) Modulus of wavelet coefficients at expansion scale 1 to 5.

Figure 20 illustrates the performance of this approach at de-noising a clinical brain PET data set reconstructed by FBP with a ramp filter. The reconstructed PET images, illustrated for one slice in Figure 20(a), contain prominent noise in high frequency but donnot express strong edge features in the wavelet modulus expansions at scale 1 through 5 as illustrated in Figure 20(b)~(f).

Cross-scale Regularization for Images with low SNR

As shown in Figure 20(b), very often in tomographic images, the first level of expansion (level with more detailed information) is overwhelmed by noise in a random pattern. Thresholding operators determined only by the information in this multi-scale level can hardly recover useful signal features from the noisy observation. On the other hand, wavelet coefficients in the first

level contain the most detailed information in a spatial-frequency expansion, and therefore influence directly the spatial resolution of the reconstructed image.

To have more signal-related coefficients recovered, additional information or *a priori* knowledge is needed. Intuitively, an edge indication map could beneficially assist such wavelet expansion based on first derivative of spline wavelets. Without seeking external *a priori* information, it was observed that wavelet modulus from the next higher wavelet level can serve as a good edge estimation. An edge indication map with values between 0 and 1 (analogous to the probability that a pixel is located on an edge) was therefore constructed by normalizing the modulus of this sub-band. A pixel-wise multiplication of the edge indication map and the first level wavelet modulus can identify the location of wavelet coefficients that are more likely to belong to a true anatomical edge and should be preserved, as well as the locations of the wavelet coefficients that are unlikely to be related to real edge signal and that should be attenuated. This approach is referred to as cross-scale regularization. A comparison between traditional wavelet shrinkage and cross-scale regularization to recover useful signals from the most detailed level of wavelet modulus is provided in Figure 21.

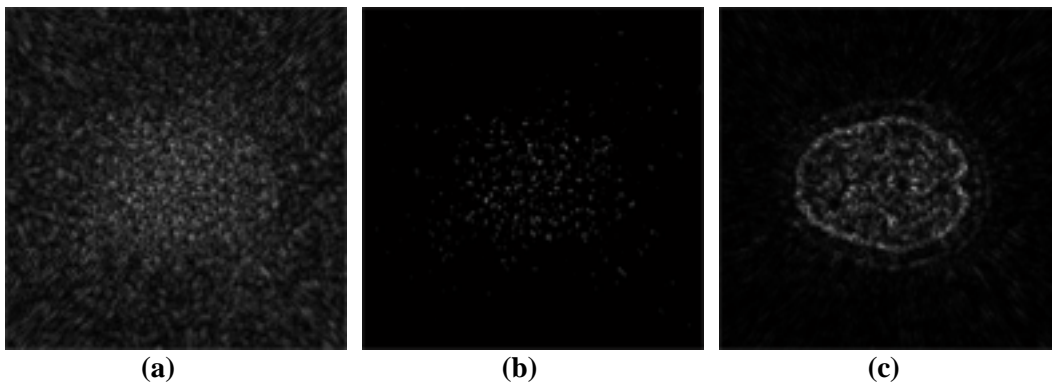


Figure 21: (a) wavelet modulus in first level of a PET brain image as shown in Figure 20 (a) and (b). (b) Thresholding of the wavelet modulus from (a) using a wavelet shrinkage operator. (c) Thresholding of the wavelet modulus from (a) with cross-scale regularization.

A cross-scale regularization process does not introduce any additional parameter avoiding extra complexity for algorithm optimization and automation. We point out that an improved edge indication prior can be built upon a modified wavelet modulus in the next spatial-frequency scale processed using traditional thresholding and enhancement operator.

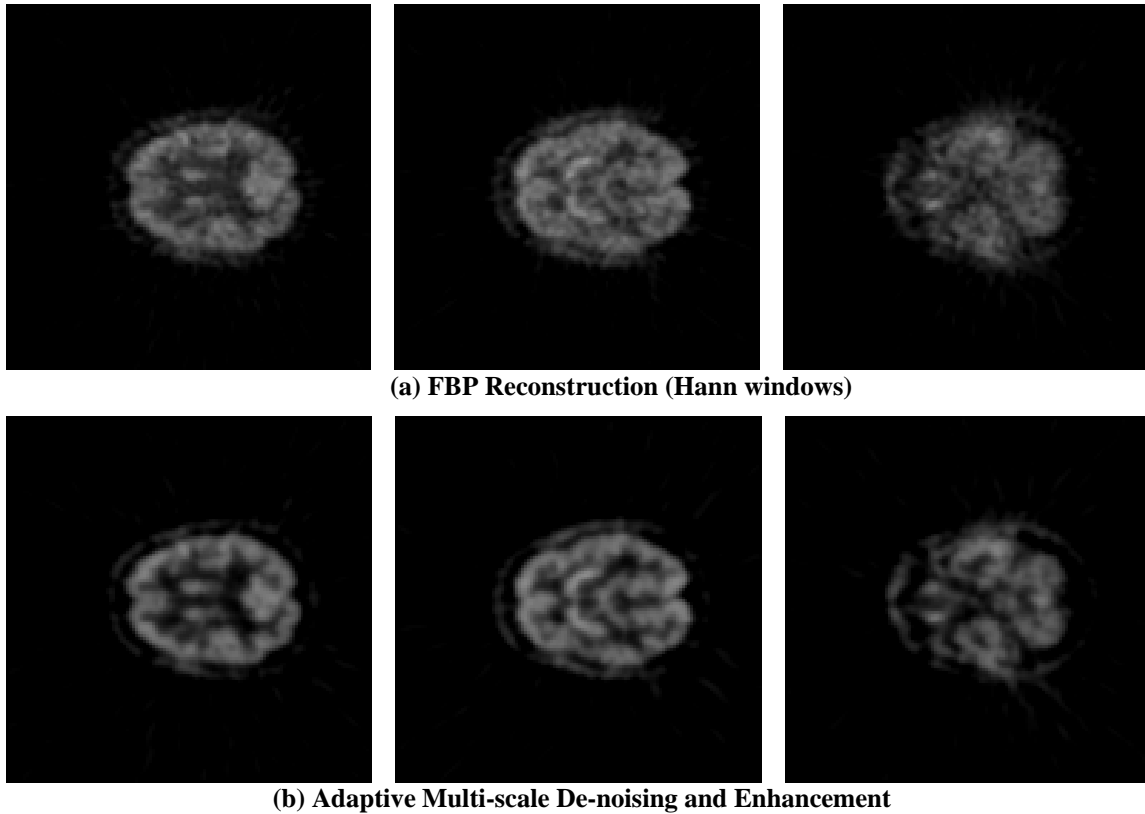


Figure 22: De-noising of PET Brain Data and comparison between unprocessed and multi-scale processed images.

Spatial-frequency representations of a signal after wavelet expansion offer the possibility to adaptively process an image data in different sub-bands. Such adaptive scheme can for example combine enhancement of wavelet coefficients in the coarse levels, and resetting of the most detailed levels for noise suppression. We show in Figure 22 how such adaptive processing can remarkably improve image quality for PET images that were usually degraded by low resolution and high level of noise.

4. Image Segmentation Using Wavelets

4.1 Multi-scale Texture Classification and Segmentation:

Texture is an important characteristic for analyzing many types of images, including natural scenes and medical images. With the unique property of spatial-frequency localization, wavelet functions provide an ideal representation for texture analysis. Experimental evidence on human and mammalian vision support the notion of spatial-frequency analysis that maximizes a simultaneous localization of energy in both spatial and frequency domain {jin_Beck_1987; jin_Julez_1981; jin_Watson_1983}. These psychophysical and physiological findings lead to several research works on texture-based segmentation methods based on multi-scale analysis.

Gabor transform, as suggested by the uncertainty principle, provides an optimal joint resolution in the space-frequency domain. Many early works utilized Gabor transforms for texture characteristics. In {jin_Daugman_1988} an example is given on the use of Gabor coefficient spectral signatures {jin_Daugman_1985} to separate distinct textural regions characterized by different orientations and predominant anisotropic texture moments. Porat and Zeevi proposed in {jin_Porat_1989} six features derived from Gabor coefficients to characterize a local texture component in an image: the dominant localized frequency; the second moment (variance) of the localized frequency; center of gravity; variance of local orientation; local mean intensity; and variance of the intensity level. A simple minimum-distance classifier was used to classify individual textured regions within a single image using these features.

Many wavelet-based texture segmentation methods had been investigated thereafter. Most of these methods follow a three-step procedure: multi-scale expansion, feature characterization, and classification. As such, they are usually different from each other from these aspects.

Various multi-scale representations have been used for texture analysis. Unser {jin_Unser_1995a} used a redundant wavelet frame. Laine and Fan {jin_Laine_1993} investigated a wavelet packets

representation and extended their research to a redundant wavelet packets frame with Lemarié-Battle filters in {jin_Laine_1996a}. Modulated wavelets were used in {jin_Hsin_1998} for better orientation adaptivity. To further extend the flexibility of the spatial-frequency analysis, a multi-wavelet packets, combining multiple wavelet basis functions at different expansion levels was used in {jin_Wang_2002}. An M -band wavelet expansion, which differs from a dyadic wavelet transform in the fact that each expansion level contains M channels of analysis was used in {jin_Acharyya_2002} to improve orientation selectivity.

Quality and accuracy of segmentation ultimately depends on the selection of the characterizing features. A simple feature selection can use the amplitude of the wavelet coefficients {jin_Hsin_1998}. Many multi-scale texture segmentation methods construct the feature vector from various local statistics of the wavelet coefficients, such as its local variance {jin_Unser_1995a; jin_Wang_2001}, moments {jin_Etemad_1997} or energy signature {jin_Acharyya_2002; jin_Laine_1993; jin_Porter_1996}. Wavelet extrema density (WED), defined as the number of extrema of wavelet coefficients per unit area, was used in {jin_Wang_2002}. In {jin_Laine_1996a}, a 1-D envelope detection was first applied to the wavelet packets coefficients according to their orientation, and a feature vector was constructed as the collection of envelope values for each spatial-frequency component. More sophisticated statistical analysis involving Bayesian analysis and Markov random fields were also used to estimate local and long-range correlations {jin_Choi_2001; jin_Zhang_1998}. For other examples of multi-scale textural features, χ^2 test and histogram testing were used in {jin_Li_2000}, “Roughness” based on fractal dimension measurement was used in {jin_Charalampidis_2002}.

Texture-based segmentation is usually achieved by texture classification. Classic classifiers such as the minimum distance classifier {jin_Porat_1989}, are easier to implement when the dimension of the feature vector is small and the groups of samples are well segregated. The most

popular classification procedures reported in the literature are the K-mean classifier {jin_Acharyya_2002; jin_Charalampidis_2002; jin_Hsin_1998; jin_Laine_1996a; jin_Porter_1996; jin_Unser_1995a; jin_Wang_2001} and the neural networks classifiers {jin_Daugman_1988; jin_Etemad_1997; jin_Laine_1993; jin_Zhang_1998}.

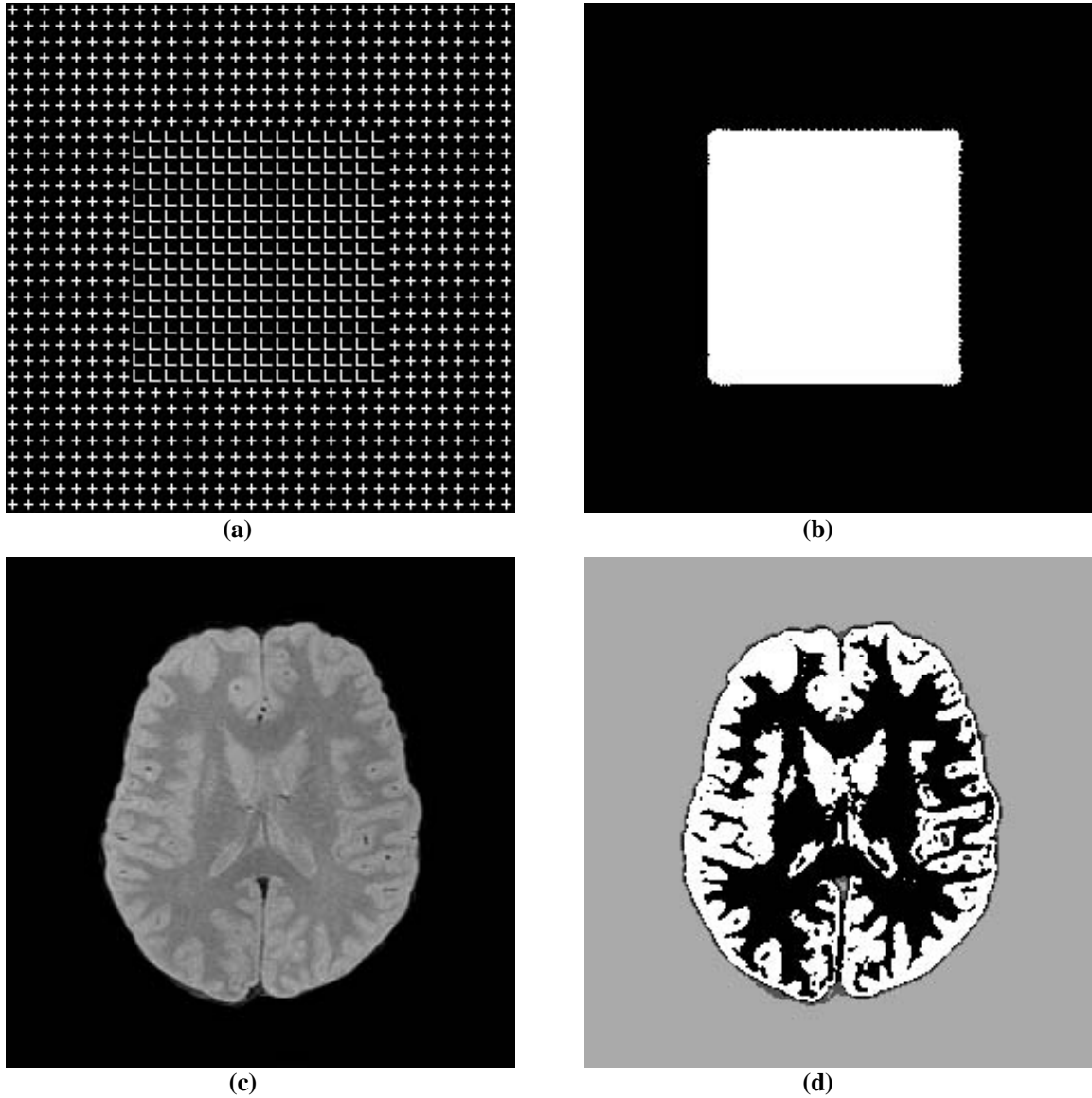


Figure 23: Sample results using multi-scale texture segmentation. (a) Synthetic texture image. (b): segmentation result for image (a) with a 2-class labeling. (c) MRI T1 image of a human brain. (d) segmentation result for image (c) with a 4-class labeling.

As an example, we illustrate in Figure 23 a texture-based segmentation method on both a synthetic texture image and a medical image from a brain MRI data set. The algorithm used for this example from {jin_Laine_1996a} uses the combination of *wavelet packets frame* with Lemarié-Battle filters, *multi-scale envelope* features, and a *K-mean* classifier.

4.2 Wavelet Edge Detection and Segmentation

Edge detection plays important role in image segmentation. In many cases, boundary delineation is the ultimate goal for an image segmentation and a good edge detector itself can then fulfill the requirement of segmentation. On the other hand, many segmentation techniques require an estimation of object edges for their initialization. For example, with standard gradient-based deformable models, an edge map is used to determine where the deforming interface must stop. In this case, the final result of the segmentation method depends heavily on the accuracy and completeness of the initial edge map. Although many research works have made some efforts to eliminate this type of inter-dependency by introducing non-edge constraints {jin_Chan_2001; jin_Yezzi_1999}, it is necessary and equally important to improve the edge estimation process itself.

As pointed out by the pioneer work of Mallat and Zhong {jin_Mallat_1992b}, first or second derivative based wavelet functions can be used for multi-scale edge detection. Most multi-scale edge detectors smooth the input signal at various scales and detect sharp variation locations (edges) from their first or second derivatives. Edge locations are related to the extrema of the first derivative of the signal and the zero crossings of the second derivative of the signal. In {jin_Mallat_1992b}, it was also pointed out that first derivative wavelet functions are more appropriate for edge detection since the magnitude of wavelet modulus represents the relative “strength” of the edges, and therefore enable to differentiate meaningful edges from small fluctuations caused by noise.

Using the first derivative of a smooth function $\theta(x, y)$ as the mother wavelet of a multi scale expansion results in a representation where the two components of wavelet coefficients at a certain scale s are related to the gradient vector of the input image $f(x, y)$ smoothed by a dilated version of $\theta(x, y)$ at scale s .

$$\begin{pmatrix} W_s^1 f(x, y) \\ W_s^2 f(x, y) \end{pmatrix} = s \bar{\nabla} (f * \theta_s)(x, y). \quad (45)$$

The direction of the gradient vector at a point (x, y) indicates the direction in the image plane along which the directional derivative of $f(x, y)$ has the largest absolute value. Edge points (local maxima) can be detected as points (x_0, y_0) such that the modulus of the gradient vector is maximum in the direction towards which the gradient vector points in the image plane. Such computation is closely related to a Canny edge detector {jin_Canny_1986}. Extension to higher dimension is quite straightforward.

Figure 24 provides an example of a multi-scale edge detection method based on a first derivative wavelet function.

To further improve the robustness of such multi-scale edge detector, Mallat and Zhong {jin_Mallat_1992b} also investigated the relations between singularity (Lipschitz regularity) and the propagation of multi-scale edges across wavelet scales. In {jin_Aydin_1996}, the dyadic expansion was extended to an M -band expansion to increase directional selectivity. Also, continuous scale representation was used for better adaptation to object sizes {jin_Laine_1997}. Continuity constraints were applied to fully recover a reliable boundary delineation from 2D and 3D cardiac ultrasound in {jin_Laine_1996b} and {jin_Koren_1994}. In {jin_Dima_2002}, both cross-scale edge correlations and spatial continuity were investigated to improve the edge detection in the presence of noise. Wilson *et al.* in {jin_Wilson_1992} also suggested that a multi-resolution Markov model can be used to track boundary curves of objects from a multi-scale expansion using a generalized wavelet transform.

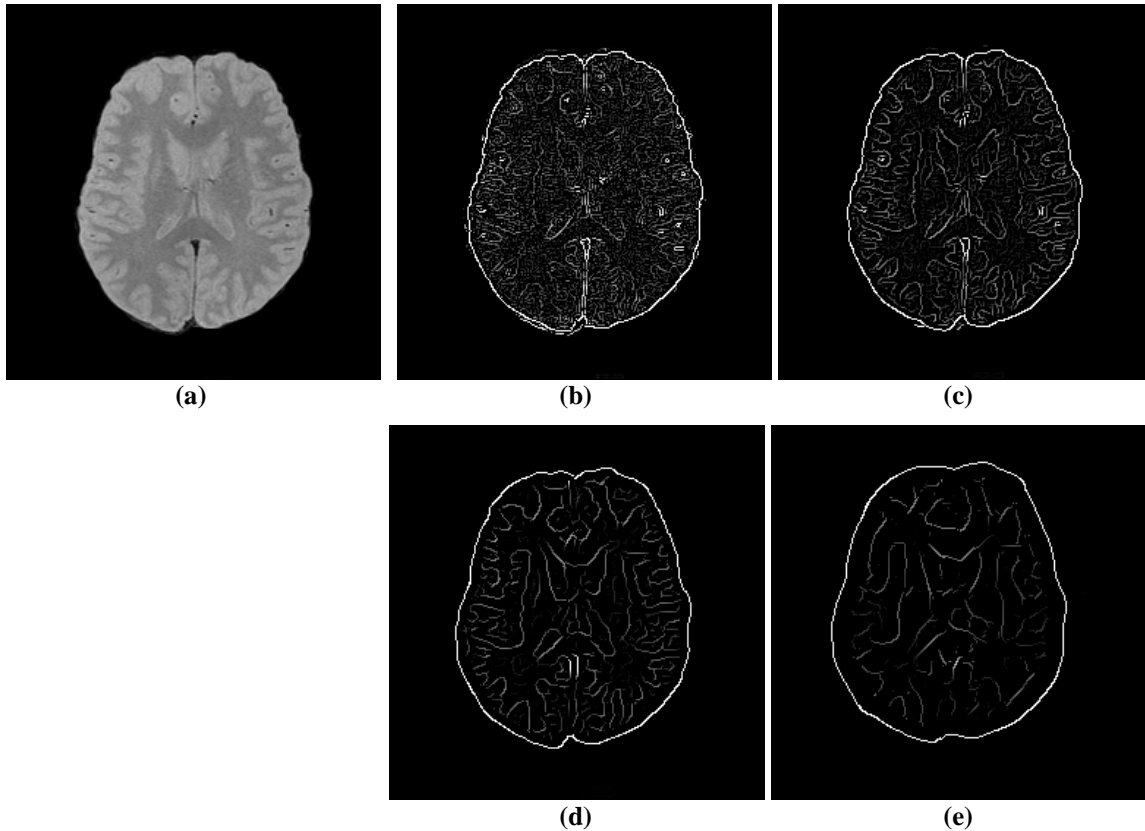


Figure 24: Example of a multi-scale edge detection method finding local maxima of wavelet modulus, with a first-derivative wavelet function. (a) Input image, (b)~(e): Multi-scale edge map at expansion scale 1 to 4.

Given their robustness and natural representation as boundary information within a multi-resolution representation, multi-scale edges have been used in deformable model methods to provide a more reliable constraint on the model deformation {jin_de Rivaz_2000; jin_Sun_2003; jin_Wu_2000; jin_Yoshida_1997}, as an alternative to traditional gradient based edge map. In {jin_Neves_2003}, it was used as a pre-segmentation step in order to find the markers that are used by watershed transform.

4.3 Other Wavelet-based Segmentation

One important feature of wavelet transform is its ability to provide a representation of the image data in a multi-resolution fashion. Such hierarchical decomposition of the image information

provides the possibility of analyzing the coarse resolution first, and then sequentially refine the segmentation result at more detailed scales. In general, such practice provides additional robustness to noise and local maxima.

In {jin_Bello_1994}, image data was first decomposed into “channels” for a selected set of resolution levels using a wavelet packets transform. A Markov random field (MRF) segmentation was then applied to the sub-bands coefficients for each scale, starting with the coarsest level, and propagating the segmentation result from one level to initialize the segmentation at the next level.

More recently, Davatzikos *et al.* {jin_Davatzikos_2003} proposed a hierarchical active shape models where the statistical properties of the wavelet transform of a deformable contour were analyzed via principal component analysis (PCA), and used as priors for constraining the contour deformations.

Many research works beneficially used image features within a spatial-frequency domain after wavelet transform to assist the segmentation. In {jin_Strickland_1996}. Strickland *et al.* used image features extracted in the wavelet transform domain for detection of microcalcifications in mammograms using a matching process and some *a priori* knowledge on the target objects (microcalcification). In {jin_Zhang_2001}, Zhang *et al.* used a Bayes classifier on wavelet coefficients to determine an appropriate scale and threshold that can separate segmentation targets from other features.

5. Image Registration Using Wavelets

In this sub-section, we give a brief overview of another very important application of wavelets in image processing: image registration. Readers with more interest in this topic are encouraged to read the references listed in the context.

Image registration is required for many image processing applications. In medical imaging, co-registration problems are important for many clinical tasks:

1. Multi-modalities study.
2. Cross-subject normalization and template/atlas analysis.
3. Patient monitoring over time with tracking of the pathological evolution for the same patient and the same modality.

Many registration methods follow a feature matching procedure. Feature points (often referred to as “control points”, or CP) are first identified in both the reference image and the input image. An optimal spatial transformation (rigid or non-rigid) is then computed that can connect and correlate the two sets of control points with minimal error. Registration has always been considered as very costly in terms of computational load. Besides, when the input image is highly deviated from the reference image, the optimization process can be easily trapped into local minima before reaching the correct transformation mapping. Both issues can be alleviated by embedding the registration into a “coarse to fine” procedure. In this framework, the initial registration is carried out on a relatively low resolution image data, and sequentially refined to higher resolution. Registration at higher resolution is initialized with the result from the lower resolution, and only need to refine the mapping between the two images with local deformations for updating the transformation parameters.

The powerful representation provided by the multi-resolution analysis framework with wavelet functions have lead many researchers to use a wavelet expansion for such “coarse to fine” procedures {jin_Allen_1993; jin_McGuire_2000; jin_Unser_1995b}. As already discussed previously, the information representation in the wavelet transform domain offers a better characterization of key spatial features and signal variations. In addition to a natural framework for “coarse to fine” procedure, many research works also reported the advantages of using wavelet sub-bands for feature characterization. For example, {jin_Zheng_1993} Zheng *et al.* constructed a set of feature points from a Gabor wavelet model that represented local curvature discontinuities. They further required that a feature point should have maximum energy among a

neighborhood and above a certain threshold. In {jin_Moigne_2002}, Moigne *et al.* used wavelet coefficients with magnitude above 13%~15% of the maximum value to form their feature space. In {jin_Dinov_2002}, Dinov *et al.* applied a frequency adaptive thresholding (shrinkage) to the wavelet coefficients to keep only significant coefficients in the wavelet transform domain for registration.

6. Summary

This chapter provided an introduction to the fundamentals of multi-scale transform theory using wavelet functions. The versatility of these multi-scale transforms make them a suitable tool for several applications in signal and image processing that can benefit from the following advantages:

1. A wavelet transform decomposes a signal to a hierarchy of sub-bands with sequential decrease in resolution. Such expansions are especially useful when a multi-resolution representation is needed. Some image segmentation and registration techniques can benefit from a “coarse to fine” paradigm based on a multi-resolution framework.
2. A signal can be analyzed with a multi-resolution framework into a spatial-frequency representation. By carefully selecting the wavelet function and the space-frequency plane tiling of the transform, distinct components from a noisy observation signal can be easily separated based on their spatial-frequency characteristics.
3. Many important features from an image data can be characterized more efficiently in the spatial-frequency domain. Such feature characterization was shown to be extremely useful in many applications including registration and data compression.

We summarized in this chapter some important applications in medical image processing using wavelet transforms. Noise reduction and enhancement can be easily implemented by combining some very simple linear thresholding techniques with wavelet expansion. Efficient de-noising and enhancement improve image quality for further analysis including segmentation and registration.

Feature characteristics in wavelet domain were proven to be potentially more efficient and reliable when compared to spatial analysis only, and therefore provided more effective segmentation and registration algorithms. We point out that many other important applications of multi-resolution wavelet transforms, that were beyond the scope of this book, have not been covered in this chapter, especially image compression, which is considered as one of the greatest achievement of wavelet transform in recent years {jin_Unser_2003b}. Other important applications include tomographic image reconstruction, analysis of functional MRI images (fMRI), and data encoding for MRI acquisition.

Despite the great success of multi-resolutions wavelet transform in medical imaging applications for the past twenty years, it continues to be a very active area of research. We list a few resources below that are of interest to readers willing to get more knowledgeable in research and applications in this area.

Conference

SPIE - The International Society for Optical Engineering, has been offering for several years two annual dedicated conferences related to wavelet applications:

1. *Wavelets: Applications in Signal and Image Processing*. (1993 - current)
2. *Independent Component Analyses, Wavelets, and Neural Networks*. (previously *Wavelet Application*.)

These conferences are held annually during the SPIE Annual Meeting and AeroSense conference.

Software

1. *Wavelet Toolbox for MATLAB*: commercial package included in MATLAB. (<http://www.mathworks.com>)
2. *Wavelab*: free MATLAB package for wavelet. (<http://www-stat.stanford.edu/~wavelab>)
3. *The Rice Wavelet Tools*: MATLAB toolbox for filter bank and wavelets provided by Rice University. (<http://www.dsp.ece.rice.edu/software/>)

4. *WVLT*: a wavelet library written in C, which also includes demos and documentation. (<http://www.cs.ubc.ca/nest/imager/contributions/bobl/wvlt/top.html>)
5. *LastWave*: a wavelet signal and image processing environment, written in C for X11/Unix and Macintosh platforms. It mainly consists of a powerful command line language with MATLAB-like syntax which includes a high level object-oriented graphic language. (<http://www.cmap.polytechnique.fr/~bacry/LastWave/>)

Web Links

1. www.wavelet.org: offers a “wavelet digest”, an email list that reports most recent news in the wavelet community. It also offers a gallery of links to many web resources including books, software, demos, research groups and tutorials. Important future events are also listed.
2. www.multiresolution.com: includes useful documentation about multi-resolution image and data analysis. Its also proposes a software package and demos for a wide range of applications.

Study Questions:

(Q1) What is the uncertainty principle in spatial-frequency analysis? How does the “uncertainty principle” affect the selection of signal representation?

(Q2) How “redundant” is an over-complete wavelet expansion? Use an example of a three dimensional signal, with a five level decomposition using the filter bank implementation shown in Figure 5.

(Q3) What is the difference between a Gabor transform and a windowed Fourier transform using a Gaussian window?

(Q4) What is the difference between a wavelet transform and a wavelet packet transform?

(Q5) What is the advantage of temporal analysis in image de-noising.

(Q6) Why is a true 3D de-noising needed for PET/SPECT images.

(Q7) Describe the three major components for accomplishing multi-scale texture segmentation.

(Q8) Between first and second derivatives, which one is preferred for multi-scale edge detection?

(Q9) What are the two most useful aspects of wavelet transforms in image registration problems?

Reference

\bibitem{jin_Acharyya_2002}

Acharyya, M. and Kundu, M.,
Document Image Segmentation Using Wavelet Scale-Space Features.,
IEEE Trans. Circuits and Systems for Video Technology,
Vol. 12, No. 12, pp. 1117-1127, 2002.

\bibitem{jin_Aldroubi_1996}

Aldroubi, A. and Unser, M.,
Wavelets in Medicine and Biology. Boca Raton, FL: CRC, 1996.

\bibitem{jin_Allen_1993}

Allen, R., Kamangar, F., and Stokely, E.,
Laplacian and Orthogonal Wavelet Pyramid Decompositions in Coarse-to-Fine Registration.,
IEEE Trans. Signal Processing,
Vol. 41, No. 12, pp. 3536-3541, 1993.

\bibitem{jin_Angelini_2001}

Angelini, E., Laine, A., Takuma, S., Holmes, J., and Homma, S.,
LV volume quantification via spatio-temporal analysis of real-time 3D echocardiography,
IEEE Transactions on Medical Imaging,
Vol. 20, pp. 457-469, 2001.

\bibitem{jin_Antoniadis_2001}

Antoniadis, A. and Fan, J.,
Regularization of Wavelet Approximations.,
Journal of American Statistics Association,
Vol. 96, No. 455, pp. 939-967, 2001.

\bibitem{jin_Aydin_1996}

Aydin, T., Yemez, Y., Anarim, E., and Sankur, B.,
Multi-directional and Multi-scale Edge Detection via M-Band Wavelet Transform.,
IEEE Trans. Image Processing,
Vol. 5, No. 9, pp. 1370-1377, 1996.

\bibitem{jin_Babaud_1986}

Babaud, J., Witkin, A., Baudin, M., and Duba, R.,
Uniqueness of the Gaussian Kernel for Scale-space Filtering.,
IEEE Trans. Pattern Analysis and Machine Intelligence,
Vol. 8, pp. 26-33, 1986.

\bibitem{jin_Bastiaans_1981}

Bastiaans, M.,
A Sampling Theorem for the Complex Spectrogram and Gabor's Expansion of a Signal in
Gaussian Elementary Signals.,
Optical Engineering,
Vol. 20, No. 4, pp. 594-598, 1981.

\bibitem{jn_Beck_1987}

Beck, J., Sutter, A., and Ivry, r.,
Spatial Frequency Channels and Perceptual Grouping in Texture Segregation.,
Computer Vision, Graphics, and Image Processing,
Vol. 37, pp. 299-325, 1987.

\bibitem{jn_Bello_1994}

Bello, M.,
A Combined Markov Random Field and Wave-Packet Transform-Based Approach for Image
Segmentation.,
IEEE Trans. Image Processing,
Vol. 3, No. 6, pp. 834-846, 1994.

\bibitem{jn_Candes_1999a}

Candes, E. and Donoho, D.,
Curvelets - A Surprisingly Effective Nonadaptive Representation for Objects with Edges.
in Curve and Surface Fitting: Saint-Malo 1999, Cohen, A., Rabut, C., and Schumaker, L., Eds.
Nashville TN: Vanderbilt University Press, 1999a.

\bibitem{jn_Candes_1999b}

Candes, E. and Donoho, D.,
Ridgelets: The Key to Higher-dimensional Intermittency?,
Phil. Trans. R. Soc. Lond. A.,
Vol. 357, pp. 2495-2509, 1999b.

\bibitem{jn_Canny_1986}

Canny, J.,
A computational approach to edge detection,
IEEE Transactions on Pattern Analysis and Machine Intelligence,
Vol. 8, No. 6, pp. 679-698, 1986.

\bibitem{jn_Chan_2001}

Chan, T. F. and Vese, L. A.,
Active Contours Without Edges,
IEEE Transactions on Image Processing,
Vol. 10, No. 2, pp. 266-277, 2001.

\bibitem{jn_Chang_2000}

Chang, S., Yu, B., and Vetterli, M.,
Spatially adaptive wavelet thresholding with context modeling for image denoising,
IEEE Transactions on Image Processing,
Vol. 9, No. 9, pp. 1522-1531, 2000.

\bibitem{jn_Charalampidis_2002}

Charalampidis, D. and Kasparis, T.,
Wavelet-based Rotational Invariant Roughness Features for Texture Classification and
Segmentation.,
IEEE Trans. Image Processing,
Vol. 11, No. 8, pp. 825-837, 2002.

\bibitem{jn_Chen_2001}

Chen, C., Lu, H., and Han, K.,
A Textural Approach Based on Gabor Functions for Texture Edge Detection in Ultrasound
Images.,
Ultrasound in Medicine and Biology,
Vol. 27, No. 4, pp. 515-534, 2001.

\bibitem{jin_Choi_2001}
Choi, H. and Baraniuk, R.,
Multiscale Image Segmentation Using Wavelet-Domain Hidden Markov Models.,
IEEE Trans. Image Processing,
Vol. 10, No. 9, pp. 1309-1321, 2001.

\bibitem{jin_Coifman_1995a}
Coifman, R. and Donoho, D.,
Translation-invariant De-noising.
in Wavelets and Statistics, Antoniadis, A. and Oppenheim, G., Eds. New York NY: Springer-
Verlag, 1995a.

\bibitem{jin_Coifman_1992}
Coifman, R. R., Meyer, Y., and Wickerhauser, M. V.,
Wavelet Analysis and signal processing
in Wavelets and their applications, Ruskai, B., Ed. Boston: Jones and Barlett, pp. 153-178, 1992.

\bibitem{jin_Coifman_1995b}
Coifman, R. R. and Woog, L. J.,
Adapted waveform analysis, wavelet packets, and local cosine libraries as a tool for image
processing,
Investigative and trial image processing, San Diego, California,
Vol. 2567, 1995b.

\bibitem{jin_Daubechies_1988}
Daubechies, I.,
Orthonormal bases of compactly supported wavelets,
Communications on Pure and Applied Mathematics,
Vol. 41, No. 7, pp. 909-996, 1988.

\bibitem{jin_Daubechies_1992}
Daubechies, I.,
Ten Lectures on Wavelets. Philadelphia, PA: Siam, 1992.

\bibitem{jin_Daugman_1985}
Daugman, J.,
Image Analysis by local 2-D Spectral Signatures.,
Journal of Optical Society of American, A,
Vol. 2, pp. 74, 1985.

\bibitem{jin_Daugman_1988}
Daugman, J.,
Complete Discrete 2-D Gabor Transforms by Neural Networks for Image Analysis and
Compression.,
IEEE Trans. Acoustics, Speech, and Signal Processing,

Vol. 36, No. 7, pp. 1169-1179, 1988.

\bibitem{jn_Davatzikos_2003}

Davatzikos, C., Tao, X., and Shen, D.,
Hierarchical Active Shape Models Using the Wavelet Transform.,
IEEE Trans. Medical Imaging,
Vol. 22, No. 3, pp. 414-423, 2003.

\bibitem{jn_de Rivaz_2000}

de Rivaz, P. and Kingsbury, N.,
Fast Segmentation Using Level Set Curves of Complex Wavelet Surfaces.,
IEEE International Conference on Image Processing,
Vol. 3, pp. 29-32, 2000.

\bibitem{jn_Dima_2002}

Dima, A., Scholz, M., and Obermayer, K.,
Automatic Segmentation and Skeletonization of Neurons From Confocal Microscopy Images
Based on the 3-D Wavelet Transform.,
IEEE Trans. Image Processing,
Vol. 11, No. 7, pp. 790-801, 2002.

\bibitem{jn_Dinov_2002}

Dinov, I., Mega, M., Thompson, P., Woods, R., Sumners, D., Sowell, E., and Toga, A.,
Quantitative Comparison and Analysis of Brain Image Registration Using Frequency-Adaptive
Wavelet Shrinkage.,
IEEE Trans. Information Technology in Biomedicine,
Vol. 6, No. 1, pp. 73-85, 2002.

\bibitem{jn_Donoho_1994a}

Donoho, D. and Johnstone, I.,
Ideal Spatial Adaptation via Wavelet Shrinkage.,
Biometrika,
Vol. 81, pp. 425-455, 1994a.

\bibitem{jn_Donoho_1995a}

Donoho, D.,
Nonlinear solution of linear inverse problems by wavelet-vaguelette decompositions,
Journal of Applied and Computational Harmonic Analysis,
Vol. 2, No. 2, pp. 101-126, 1995a.

\bibitem{jn_Donoho_1995b}

Donoho, D.,
De-noising by Soft-thresholding.,
IEEE Trans. Information Theory,
Vol. 41, No. 3, pp. 613-627, 1995b.

\bibitem{jn_Donoho_1995c}

Donoho, D. and Johnstone, I.,
Adapting to Unknown Smoothness via Wavelet Shrinkage.,
Journal of American Statistics Association,
Vol. 90, No. 432, pp. 1200-1224, 1995c.

\bibitem{jn_Donoho_1994b}

Donoho, D. L. and Johnstone, I. M.,
Ideal denoising in an orthonormal basis chosen from a library of bases,
Statistics Department, Stanford University, Technical Report 1994b.

\bibitem{jn_Etemad_1997}

Etemad, K., Doermann, D., and Chellappa, R.,
Multiscale Segmentation of Unstructured Document Pages Using Soft Decision Integration.,
IEEE Trans. Pattern Analysis and Machine Intelligence,
Vol. 19, No. 1, pp. 92-96, 1997.

\bibitem{jn_Fan_1996}

Fan, J. and Laine, A.,
Multi-scale Contrast Enhancement and De-noising in Digital Radiographs.
in Wavelets in Medicine and Biology, Aldroubi, A. and Unser, M., Eds. Boca Raton FL: CRC
Press, pp. 163-189, 1996.

\bibitem{jn_Farquhar_1998}

Farquhar, T. H., Chatziioannou, A., Chinn, G., Dahlbom, M., and Hoffman, E. J.,
An investigation of filter choice for filtered back-projection reconstruction in PET,
IEEE Transactions on Nuclear Science,
Vol. 45, No. 3 Part 2, pp. 1133 - 1137, 1998.

\bibitem{jn_Feichtinger_1998}

Feichtinger, H. and Strohmer, T.,
Gabor Analysis and Algorithms: Theory and Applications, 1998.

\bibitem{jn_Freeman_1991}

Freeman, W. and Adelson, E.,
The Design and Use of Steerable Filters.,
IEEE Trans. Pattern Analysis and Machine Intelligence,
Vol. 13, pp. 891-906, 1991.

\bibitem{jn_Gabor_1946}

Gabor, D.,
Theory of Communication.,
Journal of the IEE,
Vol. 93, pp. 429-457, 1946.

\bibitem{jn_Gao_1997}

Gao, H. and Bruce, A.,
WaveShrink with Firm Shrinkage.,
Statist. Sinica,
Vol. 7, pp. 855-874, 1997.

\bibitem{jn_Gao_1998}

Gao, H.,
Wavelet Shrinkage Denoising Using the Non-negative Garrote.,
J. Comp. Graph. Statist.,
Vol. 7, pp. 469-488, 1998.

- \bibitem{jn_Grossman_1984}
 Grossman, A. and Morlet, J.,
 Decomposition of Hardy Functions into Square Integrable Wavelets of Constant Shape.,
 SIAM Journal of Mathematical Analysis,
 Vol. 15, No. 4, pp. 723-736, 1984.
- \bibitem{jn_Haar_1910}
 Haar, A.,
 Zur Theorie der Orthogonalen Funktionensysteme.,
 Math. Annal.,
 Vol. 69, pp. 331-371, 1910.
- \bibitem{jn_Holschneider_1989}
 Holschneider, M., Kronland-Martinet, K., Morlet, J., and Tchamitchian, P.,
 Wavelets, Time Frequency Methods and Phase Space. Berlin: Springer-Verlag, 1989.
- \bibitem{jn_Hsin_1998}
 Hsin, H. and Li, C.,
 An Experiment on Texture Segmentation Using Modulated Wavelets,
 IEEE Trans. System, Man and Cybernetics-Part A: System and Humans,
 Vol. 28, No. 5, pp. 720-725, 1998.
- \bibitem{jn_Hubel_1962}
 Hubel, D. and Wiesel, T.,
 Receptive Fields, Binocular Interaction and Functional Architecture in the Cat's Visual Cortex.,
 Journal of Physiology,
 Vol. 160, 1962.
- \bibitem{jn_Hudson_1994}
 Hudson, H. and Larkin, R.,
 Accelerated Image Reconstruction Using Ordered Subsets of Projection Data.,
 IEEE Trans. Medical Imaging,
 Vol. 13, No. 4, pp. 601-609, 1994.
- \bibitem{jn_Jain_1989}
 Jain, A. K.,
 Fundamentals of Digital Image Processing. Englewood Cliffs, NJ: Prentice-Hall, 1989.
- \bibitem{jn_Jansen_1997}
 Jansen, M., Malfait, M., and Bultheel, A.,
 Generalised Cross-validation for Wavelet Thresholding.,
 Signal Processing.,
 Vol. 56, pp. 33-44, 1997.
- \bibitem{jn_Jin_2003}
 Jin, Y., Angelini, E., Esser, P., and Laine, A.,
 De-noising SPECT/PET Images Using Cross-scale Regularization.,
 Proceedings of the Sixth International Conference on Medical Image Computing and Computer
 Assisted Interventions (MICCAI 2003), Montreal Canada,
 Vol. 2879, No. 2, pp. 32-40, 2003.

\bibitem{jn_Julez_1981}

Julez, B.,
A Theory of Preattentive Texture Discrimination Based on first-order Statistics of Textons.,
Biol. Cybern.,
Vol. 41, pp. 131-138, 1981.

\bibitem{jn_Kalifa_2003}

Kalifa, J., Laine, A., and Esser, P.,
Regularization in Tomographic Reconstruction Using Thresholding Estimators.,
IEEE Trans. Medical Imaging,
Vol. 22, No. 3, pp. 351-359, 2003.

\bibitem{jn_Koren_1994}

Koren, I., Laine, A. F., Fan, J., and Taylor, F. J.,
Edge detection in echocardiographic image sequences by 3-D multiscale analysis,
IEEE International Conference on Image Processing,
Vol. 1, No. 1, pp. 288-292, 1994.

\bibitem{jn_Koren_1995}

Koren, I., Laine, A., and Taylor, F.,
Image fusion using steerable dyadic wavelet transform,
Proceedings of the International Conference on Image Processing, Washington, D.C., pp. 232-235, 1995.

\bibitem{jn_Koren_1996}

Koren, I.,
A Multiscale Spline Derivative-Based Transform for Image Fusion and Enhancement,
Ph.D. Thesis, Electrical Engineering, University of Florida, 1996.

\bibitem{jn_Koren_1998}

Koren, I. and Laine, A.,
A discrete dyadic wavelet transform for multidimensional feature analysis
in Time Frequency and Wavelets in Biomedical Signal Processing, *IEEE Press series in
biomedical engineering*, Akay, M., Ed. Piscataway, NJ: IEEE Press, pp. 425-448, 1998.

\bibitem{jn_Laine_1993}

Laine, A. and Fan, J.,
Texture classification by wavelet packet signatures,
IEEE Transactions on Pattern Analysis and Machine Intelligence,
Vol. 15, No. 11, pp. 1186-1191, 1993.

\bibitem{jn_Laine_1994a}

Laine, A., Fan, J., and Schuler, S.,
A Framework for Contrast Enhancement by Dyadic Wavelet Analysis.
in Digital Mammography, Gale, A., Astley, S., Dance, D., and Cairns, A., Eds. Amsterdam, The
Netherlands: Elsevier, 1994a.

\bibitem{jn_Laine_1994b}

Laine, A., Schuler, S., Fan, J., and Huda, W.,
Mammographic Feature Enhancement by Multiscale Analysis.,

IEEE Trans. Medical Imaging,
Vol. 13, No. 4, pp. 725-740, 1994b.

\bibitem{jn_Laine_1995}
Laine, A., Fan, J., and Yang, W.,
Wavelets for Contrast Enhancement of Digital Mammography.,
IEEE Engineering in Medicine and Biology, No. September, pp. 536-550, 1995.

\bibitem{jn_Laine_1996a}
Laine, A. and Fan, J.,
Frame Representation for Texture Segmentation.,
IEEE Trans. Image Processing,
Vol. 5, No. 5, pp. 771-780, 1996a.

\bibitem{jn_Laine_1996b}
Laine, A. and Zong, X.,
Border Identification of Echocardiograms via Multiscale Edge Detection and Shape Modeling.,
IEEE International Conference on Image Processing, Lausanne, Switzerland, pp. 287-290, 1996b.

\bibitem{jn_Laine_2000}
Laine, A.,
Wavelets in spatial processing of biomedical images,
Annual Review of Biomedical Engineering,
Vol. 2, pp. 511-550, 2000.

\bibitem{jn_Laine_1997}
Laine, A. F., Huda, W., Chen, D., and Harris, J. G.,
Local enhancement of masses using continuous scale representations.,
Journal of Mathematical Imaging and Vision,
Vol. 7, No. 1, 1997.

\bibitem{jn_Li_2000}
Li, J. and Gray, R.,
Context-Based Multiscale Classification of Document Images Using Wavelet Coefficient
Distributions.,
IEEE Trans. Image Processing,
Vol. 9, No. 9, pp. 1604-1616, 2000.

\bibitem{jn_Liebling_2003}
Liebling, M., Blu, T., and Unser, M.,
Fresnels: New Multiresolution Wavelet Bases for Digital Holography.,
IEEE Trans. Image Processing,
Vol. 12, No. 1, pp. 29-43, 2003.

\bibitem{jn_Mallat_1989}
Mallat, S.,
A theory for multiresolution signal decomposition: The wavelet representation,
IEEE Transactions on Pattern Analysis and Machine Intelligence,
Vol. 11, No. 7, pp. 674-693, 1989.

\bibitem{jn_Mallat_1992a}

Mallat, S. and Hwang, W. L.,
Singularity detection and processing with wavelets,
IEEE Transactions on Information Theory,
Vol. 38, No. 2, pp. 617-643, 1992a.

\bibitem{jn_Mallat_1992b}
Mallat, S. and Zhong, S.,
Characterization of signals from multiscale edges,
IEEE Transactions on Pattern Analysis and Machine Intelligence,
Vol. 14, No. 7, pp. 710-732, 1992b.

\bibitem{jn_Mallat_1998}
Mallat, S.,
A Wavelet Tour of Signal Processing. San Diego, CA: Academic Press, 1998.

\bibitem{jn_Malvar_1990}
Malvar, H.,
Lapped transforms for efficient transform / subband coding,
IEEE trans. Acoust. Sign. Speech Process.,
Vol. 38, pp. 969-978, 1990.

\bibitem{jn_McGuire_2000}
McGuire, M. and Stone, H.,
Techniques for Multiresolution Image Registration in the Presence of Occlusions.,
IEEE Trans. Geoscience and Remote Sensing,
Vol. 38, No. 3, pp. 1476-1479, 2000.

\bibitem{jn_McLachlan_1997}
McLachlan, G. J. and Krishnan, T.,
The EM Algorithm and Extensions. New York: John and Wiley & Sons, Inc, 1997.

\bibitem{jn_Meyer_1997}
Meyer, F. and Coifman, R.,
Brushlets: A Tool for Directional Image Analysis and Image Compression.,
Applied and Computational harmonic Analysis,
Vol. 4, pp. 147-187, 1997.

\bibitem{jn_Moigne_2002}
Moigne, J., Campbell, W., and Crompton, R.,
Automated Parallel Image Registration Technique Based on the correlation of Wavelet Features.,
IEEE Trans. Geoscience and Remote Sensing,
Vol. 40, No. 8, pp. 1849-1864, 2002.

\bibitem{jn_Mulet-Parada_1998}
Mulet-Parada, M. and Noble, J. A.,
2D+T acoustic boundary detection in echocardiography,
Medical Image Computing and Computer-Assisted Intervention-MICCAI'98, Cambridge, MA,
pp. 806-813, 1998.

\bibitem{jn_Nason_1996}
Nason, G.,

Wavelet Shrinkage Using Cross-validation.,
J. R. Statist. Soc.,
Vol. 58, pp. 463-479, 1996.

\bibitem{jn_Neves_2003}
Neves, S., daSilva, E., and Mendonca, G.,
Wavelet-watershed Automatic Infrared Image Segmentation Method.,
IEEE Electronics Letters.,
Vol. 39, No. 12, pp. 903-904, 2003.

\bibitem{jn_Ogden_1996}
Ogden, R. T. and Parzen, E.,
Change-point Approach to Data Analytic Wavelet Thresholding,
Statistics and Computing,
Vol. 6, pp. 93-99, 1996.

\bibitem{jn_Papoulis_1987}
Papoulis, A.,
The Fourier Integral and its Applications. New York NY: McGraw-Hill, 1987.

\bibitem{jn_Porat_1988}
Porat, M. and Zeevi, Y.,
The Generalized Gabor Scheme of image representation in biological and machine vision,
IEEE Transactions on Pattern Analysis and Machine Intelligence,
Vol. 10, No. 4, pp. 452-468, 1988.

\bibitem{jn_Porat_1989}
Porat, M. and Zeevi, Y.,
Localized texture processing in vision: Analysis and synthesis in the Gaborian space.,
IEEE Transactions on Biomedical Engineering.,
Vol. 36, No. 1, pp. 115-129, 1989.

\bibitem{jn_Porter_1996}
Porter, R. and Canagarajah, N.,
A Robust Automatic clustering Scheme for Image Segmentation Using Wavelets.,
IEEE Trans. Image Processing,
Vol. 5, No. 4, pp. 662-665, 1996.

\bibitem{jn_Selesnick_1999}
Selesnick, I.,
The Slantlet Transform.,
IEEE Trans. Signal Processing,
Vol. 47, No. 5, pp. 1304-1313, 1999.

\bibitem{jn_Shensa_1992}
Shensa, M.,
The Discrete Wavelet Transform: Wedding the a trous and Mallat Algorithms.,
IEEE Trans. Signal Processing,
Vol. 40, No. 10, pp. 2464-2482, 1992.

\bibitem{jn_Shepp_1982}

Shepp, L. and Vardi, V.,
Maximum Likelihood Reconstruction for Emission Computed Tomography.,
IEEE Trans. Medical Imaging,
Vol. 1, pp. 113-122, 1982.

\bibitem{jn_Starck_2002}
Starck, J., Candes, E., and Donoho, D.,
The Curvelet Transform for Image Denoising.,
IEEE Trans. Image Processing,
Vol. 11, No. 6, pp. 670-684, 2002.

\bibitem{jn_Stein_1981}
Stein, C.,
Estimation of the mean of a multivariate normal distribution.,
Annals of Statistics,
Vol. 9, pp. 1135-1151, 1981.

\bibitem{jn_Strickland_1995}
Strickland, R. N. and Hahn, H. I.,
Wavelet transform matched filters for the detection and classification of microcalcifications in mammography,
Proceedings of the International Conference on Image Processing, Washington, D.C.,
Vol. 1, pp. 422-425, 1995.

\bibitem{jn_Strickland_1996}
Strickland, R. N. and Hahn, H. I.,
Wavelet transforms for detecting microcalcifications in mammograms,
IEEE Transactions on Medical Imaging,
Vol. 15, No. 2, pp. 218-229, 1996.

\bibitem{jn_Sun_2003}
Sun, H., Haynor, D., and Kim, Y.,
Semiautomatic Video Object Segmentation using VSnakes.,
IEEE Trans. Circuits and Systems for Video Technology,
Vol. 13, No. 1, pp. 75-82, 2003.

\bibitem{jn_Unser_1995a}
Unser, M.,
Texture classification and segmentation using wavelet frames,
IEEE Transactions on Image Processing,
Vol. 4, No. 11, pp. 1549-1560, 1995a.

\bibitem{jn_Unser_1995b}
Unser, M., Thevenaz, P., Lee, C., and Ruttimann, U.,
Registration and Statistical Analysis of PET Images Using the Wavelet Transform.,
IEEE Engineering in Medicine and Biology, No. September/October, pp. 603-611, 1995b.

\bibitem{jn_Unser_1996}
Unser, M. and Aldroubi, A.,
A review of wavelets in biomedical applications,
Proceedings of the IEEE,

Vol. 84, No. 4, pp. 626-638, 1996.

`\bibitem{jn_Unser_2003a}`

Unser, M., Aldroubi, A., and Laine, A.,
IEEE Transactions on Medical Imaging: Special Issue on Wavelets in Medical Imaging., 2003a.

`\bibitem{jn_Unser_2003b}`

Unser, M. and Blu, T.,
Mathematical Properties of the JPEG2000 Wavelet Filters.,
IEEE Trans. Image Processing,
Vol. 12, No. 9, pp. 1080-1090, 2003b.

`\bibitem{jn_Wang_2001}`

Wang, J., Li, J., Gray, R., and Wiederhold, G.,
Unsupervised Multiresolution Segmentation for Images with Low Depth of Field.,
IEEE Trans. Pattern Analysis and Machine Intelligence,
Vol. 23, No. 1, pp. 85-90, 2001.

`\bibitem{jn_Wang_2002}`

Wang, J.,
Multiwavelet Packet Transform with Application to Texture Segmentation.,
Electronics Letters,
Vol. 38, No. 18, pp. 1021-1023, 2002.

`\bibitem{jn_Watson_1983}`

Watson, A., Barlow, H., and Robson, J.,
What Dose the Eye See Best?,
Nature,
Vol. 302, pp. 419-422, 1983.

`\bibitem{jn_Weaver_1991}`

Weaver, J. B., Yansun, X., Healy, D. M., and Cromwell, L. D.,
Filtering noise from images with wavelet transforms,
Magnetic Resonance in Medicine,
Vol. 21, No. 2, pp. 288-295, 1991.

`\bibitem{jn_Weyrich_1995}`

Weyrich, N. and Warhola, G.,
De-noising Using Wavelets and Cross-validation.,
NATA Adv. Study Inst.,
Vol. 454, pp. 523-532, 1995.

`\bibitem{jn_Wickerhauser_1993}`

Wickerhauser, M. V.,
Adapted Wavelet Analysis from Theory to Software. Wellesley, Massachusetts, 1993.

`\bibitem{jn_Wilson_1992}`

Wilson, R., Calway, A., and Pearson, R.,
A Generalized Wavelet Transform for Fourier Analysis : The Multiresolution Fourier Transform
and its Application to Image and Audio Signal Analysis.,
IEEE Trans. on Information Theory,

Vol. 38, No. 2, pp. 674-690, 1992.

\bibitem{jn_Wu_2000}

Wu, H., Liu, J., and Chui, C.,

A Wavelet Frame Based Image Force Model for Active Contouring Algorithms.,

IEEE Trans. Image Processing,

Vol. 9, No. 11, pp. 1983-1988, 2000.

\bibitem{jn_Yezzi_1999}

Yezzi, A., Tsai, A., and Willsky, A.,

A statistical approach to image segmentation for bimodal and trimodal imagery.,

ICCV, pp. 898-903, 1999.

\bibitem{jn_Yoshida_1997}

Yoshida, H., Katsuragawa, S., Amit, Y., and Doi, K.,

Wavelet Snake for Classification of Nodules and False Positives in Digital Chest Radiographs.,

IEEE EMBS Annual Conference, Chicago IL, pp. 509-512, 1997.

\bibitem{jn_Zhang_1998}

Zhang, J., Wang, D., and Tran, Q.,

A Wavelet-Based Multiresolution Statistical Model for Texture.,

IEEE Trans. Image Processing,

Vol. 7, No. 11, pp. 1621-1627, 1998.

\bibitem{jn_Zhang_2001}

Zhang, X. and Desai, M.,

Segmentation of Bright Targets Using Wavelets and Adaptive Thresholding.,

IEEE Trans. Image Processing,

Vol. 10, No. 7, pp. 1020-1030, 2001.

\bibitem{jn_Zheng_1993}

Zheng, Q. and Chellappa, R.,

A Computational Vision Approach to Image Registration.,

IEEE Trans. Image Processing,

Vol. 2, No. 3, pp. 311-325, 1993.